先进感知系统及其信息处理

Advanced Sensing Systems with Information Processing

第四讲

授课教师：许小剑

北京航空航天大学电子信息工程学院
北航新主楼F座403室
Tel: 82316065
Email: xiaojianxu@buaa.edu.cn

2021年春季学期

第四讲 红外辐射模型

(Infrared Radiation Models)

- VNIR和SWIR谱段辐射模型
- MWIR和TIR谱段辐射模型
- 红外辐射模型的拓展：空中目标的红外辐射建模

传感器信息处理要干什么?

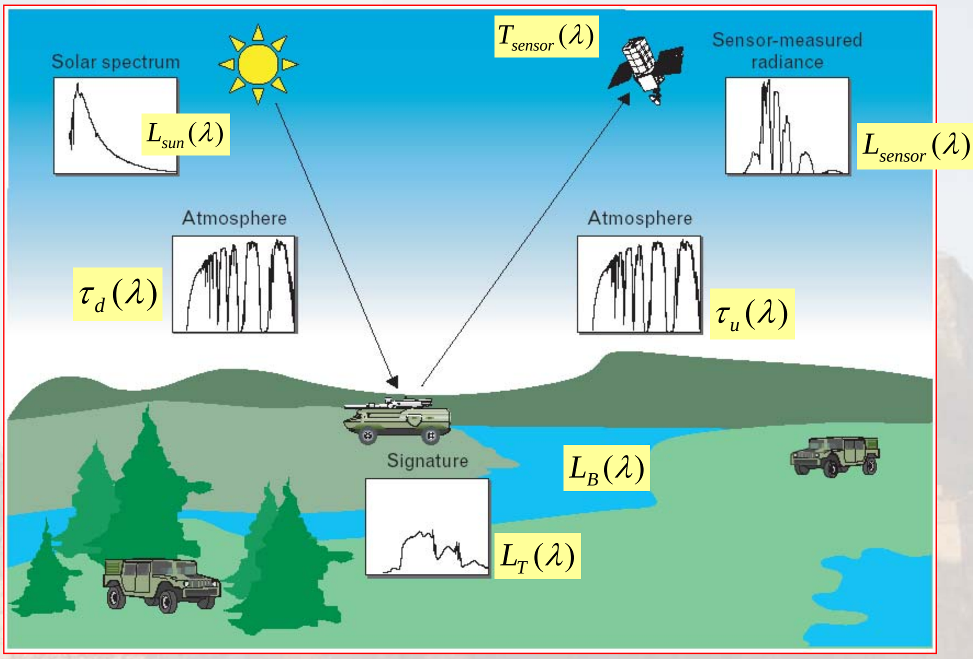

传感器得到的： $L_{sensor}(\lambda) = \{L_{sun}(\lambda) * \tau_d(\lambda) * [L_T(\lambda) + L_B(\lambda)] * \tau_u(\lambda)\} * T_{sensor}(\lambda)$

目标信息： $L_T(\lambda), L_B(\lambda) \to \rho, \varepsilon, T$

不同谱段传感器感兴趣的物理量

	name	wavelength range	radiation source	surface property of interest
VNIR	Visible (V)	0.4 – 0.7µm	solar	reflectance
	Near InfraRed (NIR)	0.7 – 1.1µm	solar	reflectance
	Short Wave InfraRed (SWIR)	1.1 – 1.35µm 1.[illegible] – 1.8µm 2 – 2.5µm	solar	reflectance
MWIR	Mid Wave InfraRed (MWIR)	3 – 4µm 4.5 – 5µm	solar, thermal	reflectance, temperature
TIR	Thermal InfraRed (TIR)	8 – 9.5µm 10 – 14µm	thermal	temperature

第四讲 红外辐射模型

(Infrared Radiation Models)

- VNIR和SWIR谱段辐射模型
- MWIR和TIR谱段辐射模型
- 红外辐射模型的拓展：空中目标的红外辐射建模

VNIR/SWIR谱段传感器所感兴趣的物理量—光谱反射率

name	wavelength range	radiation source	surface property of interest
Visible (V)	0.4 – 0.7μm	solar	reflectance
Near InfraRed (NIR)	0.7 – 1.1μm	solar	reflectance
Short Wave InfraRed (SWIR)	1.1 – 1.35μm 1.[illegible] – 1.8μm 2 – 2.5μm	solar	reflectance
Mid Wave InfraRed (MWIR)	3 – 4μm 4.5 – 5μm	solar, thermal	reflectance, temperature
Thermal InfraRed (TIR)	8 – 9.5μm 10 – 14μm	thermal	temperature
microwave, radar	1mm – 1m	thermal (passive) artificial (active)	temperature (passive) roughness (active)

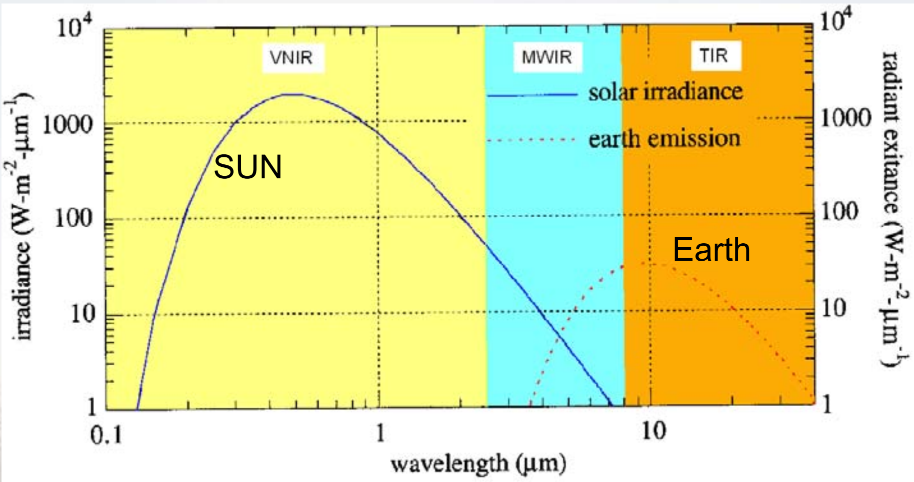

In the 0.4-3μm spectral range,

- Sun's irradiance to the earth's surface dominates
- All materials on the earth's surface passively absorb and reflect solar radiation
- Some materials also transmit solar radiation (e.g., water body, plant canopies, etc.)

Radiation Components

Three significant components in the upwelling at-sensor radiation:

- **The unscattered, surface-reflected radiation**
- **The down-scattered, surface-reflected skylight**
- **The up-scattered path radiance**

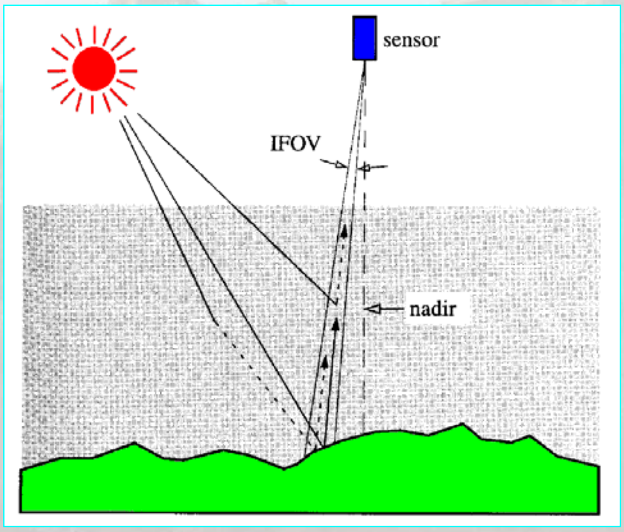

The first two are surface-reflected; while the third is path-scattered.

Surface-reflected

L_λ^{su}

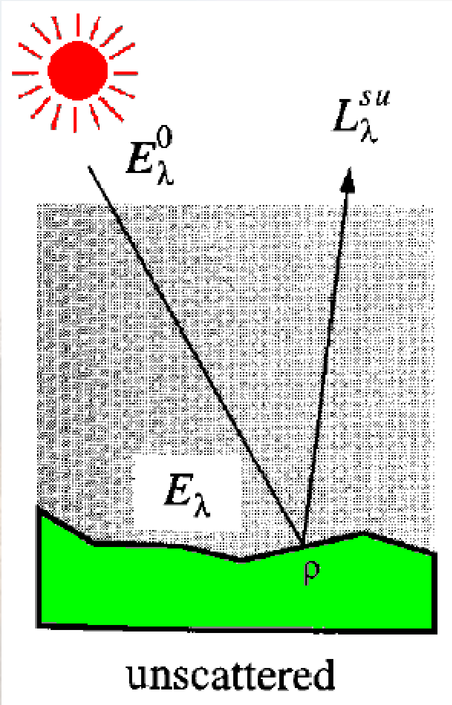

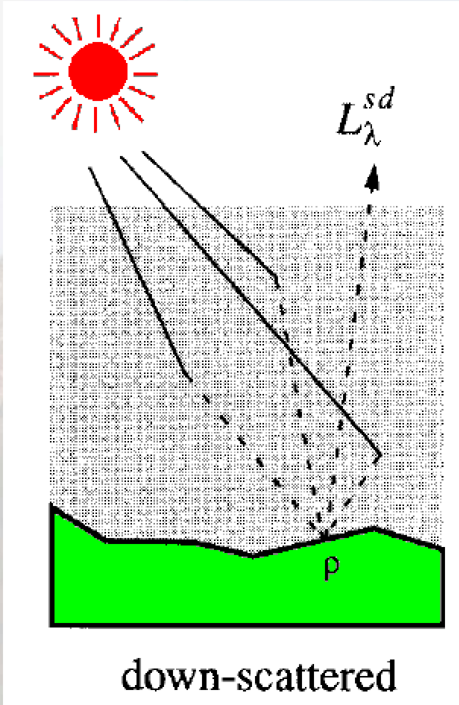

L_λ^{sd}

- **The unscattered, surface-reflected radiation**
- **The down-scattered, surface-reflected skylight**

Path-scattered radiation

L_λ^{sp}

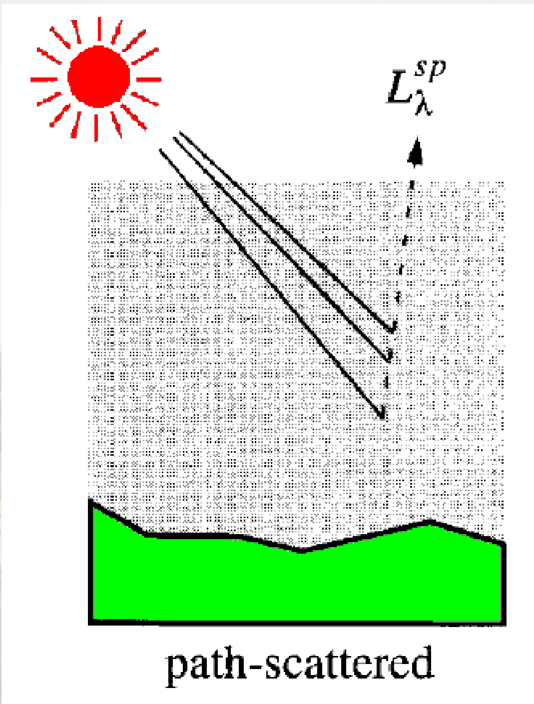

- **The up-scattered path radiance**

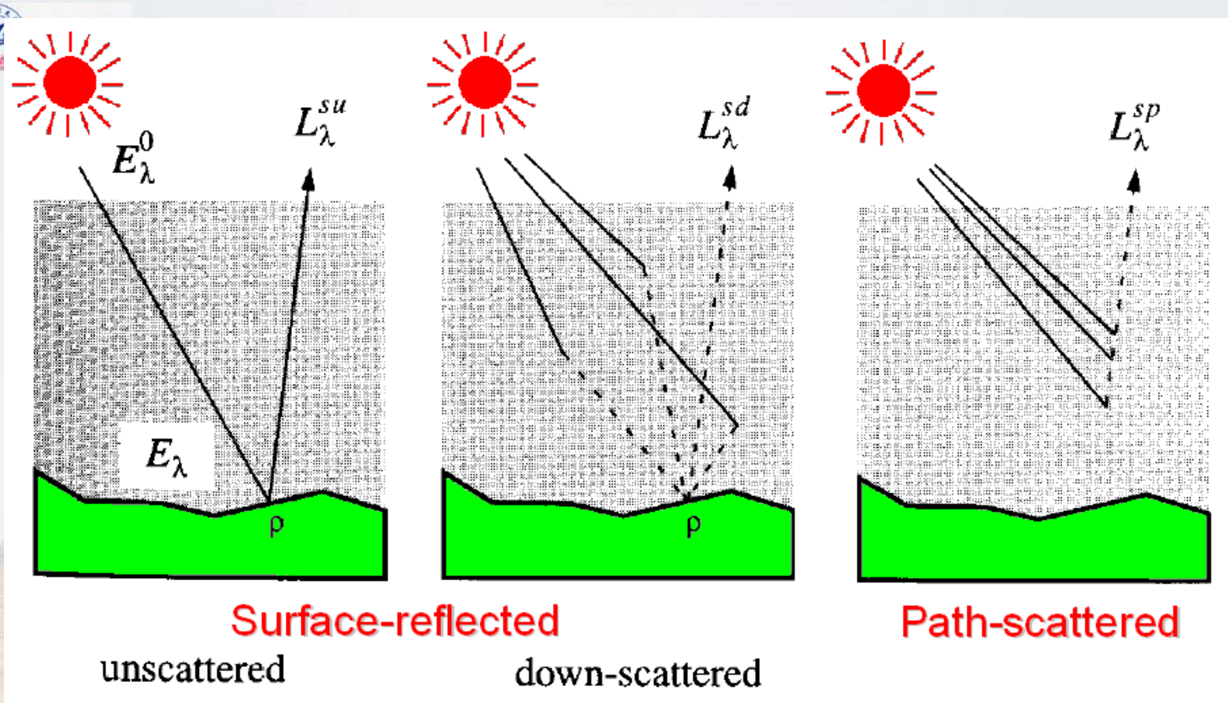

- The unscattered, surface-reflected radiation
- The down-scattered, surface-reflected skylight
- The up-scattered path radiance

$$L_\lambda^s = L_\lambda^{su} + L_\lambda^{sd} + L_\lambda^{sp}$$

The unscattered, surface-reflected radiation

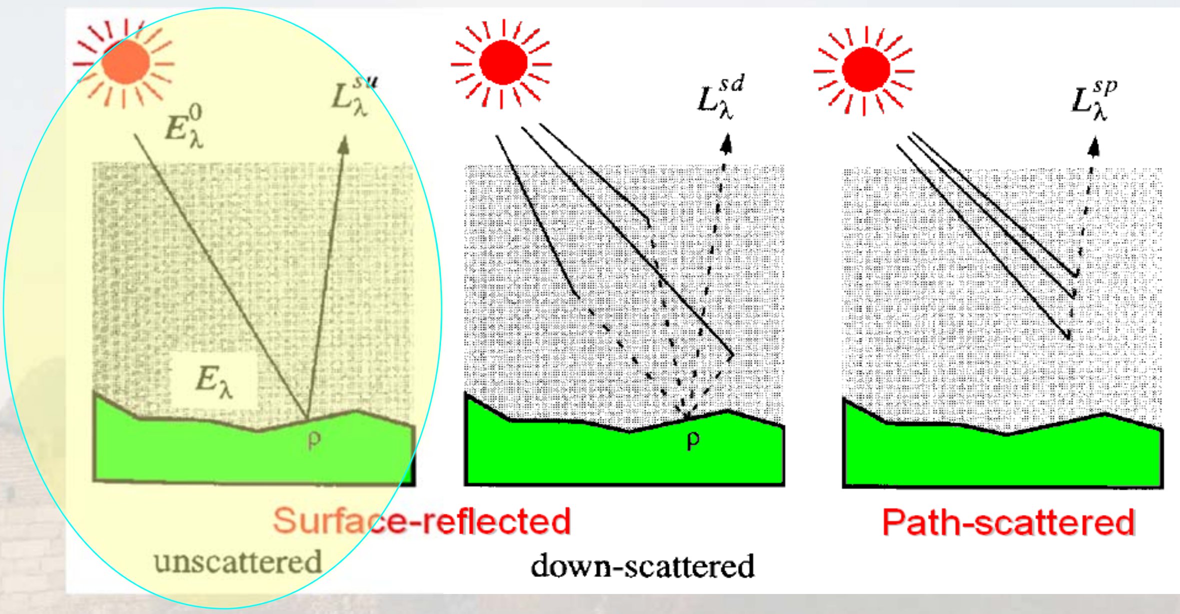

- The unscattered, surface-reflected radiation
- The down-scattered, surface-reflected skylight
- The up-scattered path radiance

$$L_\lambda^s = L_\lambda^{su} + L_\lambda^{sd} + L_\lambda^{sp}$$

The unscattered, surface-reflected radiation

$$L_\lambda^{su}$$

$$L_\lambda^{s} = L_\lambda^{su} + L_\lambda^{sd} + L_\lambda^{sp}$$

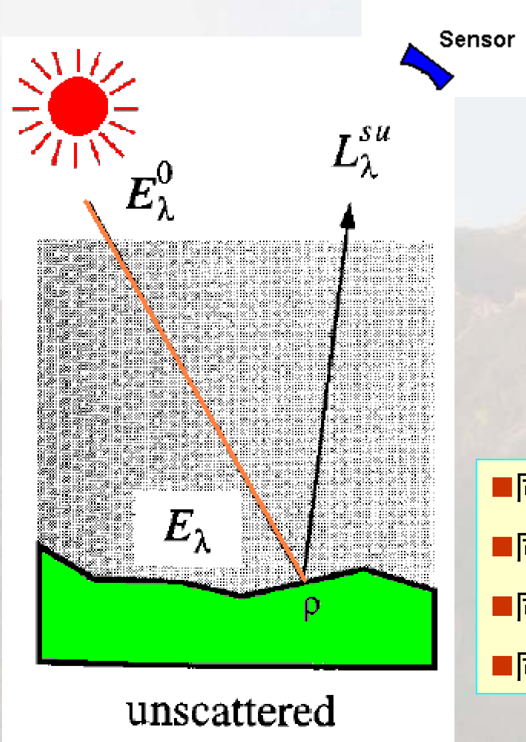

- 同太阳辐射有关
- 同大气传输有关
- 同地面有关
- 同传感器位置有关

The Sun's Radiation

Plank's Equation:

$$M_\lambda = \frac{C_1}{\lambda^5 [e^{C_2/(\lambda T)} - 1]}$$

where

T is the blackbody's temperature in Kelvin (K),
$C_1 = 3.74151 \times 10^8$ W-m^{-2}-μm^4, and
$C_2 = 1.43879 \times 10^4$ μm-K.

We are interested in the radiation that reaches the earth.

Spectral irradiance at the top of the atmosphere:

$$E_\lambda^0 = \frac{M_\lambda}{\pi} \times \frac{\text{area solar disk}}{(\text{distance-to-earth})^2}$$

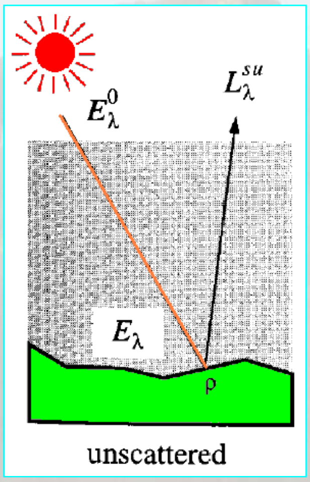

The Sun's Radiation

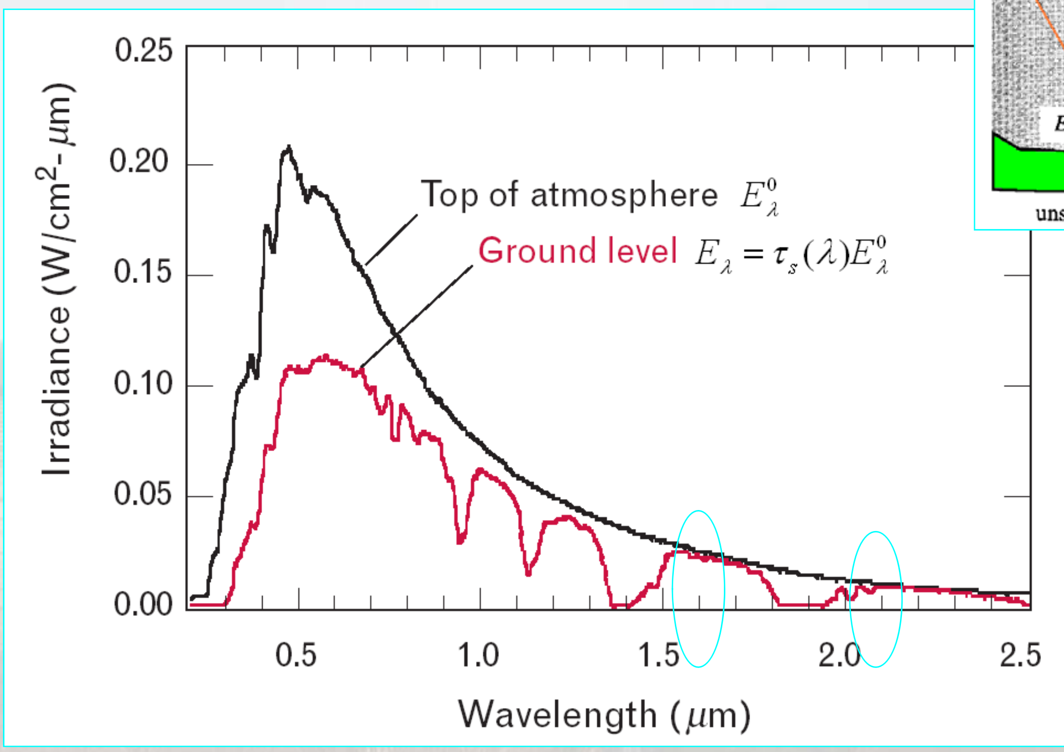

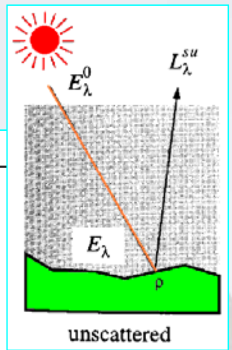

The atmospheric transmission

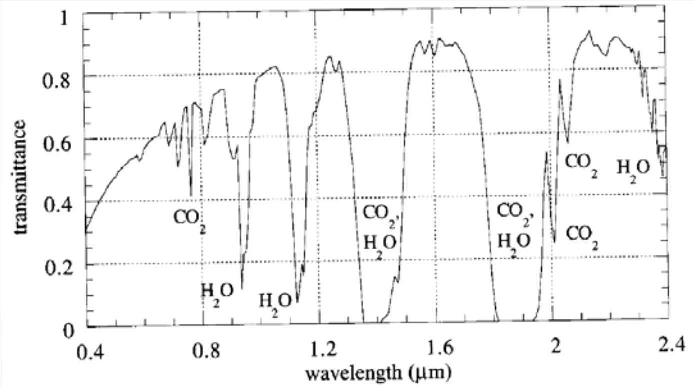

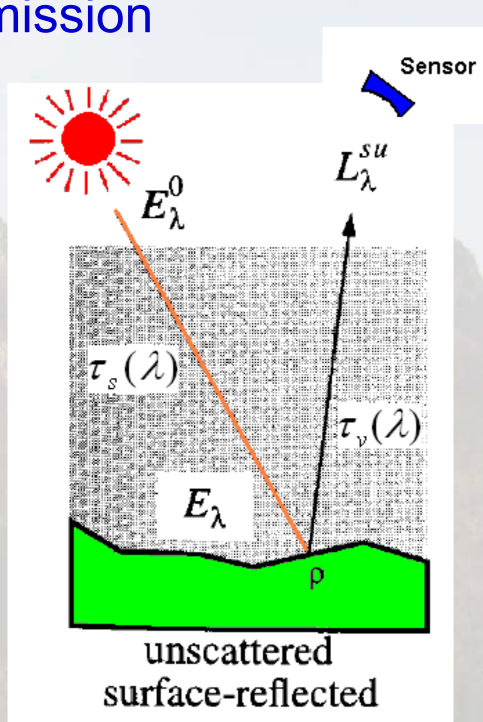

At Earth's surface, the incident spectral irradiance of the Sun is :

$$E_\lambda = \tau_s(\lambda) E_\lambda^0$$

Transmittance of Top atmosphere to the Earth surface: an example calculated by MODTRAN or any other models, such SBDART, LOWTRAN

$\tau_s(\lambda)$

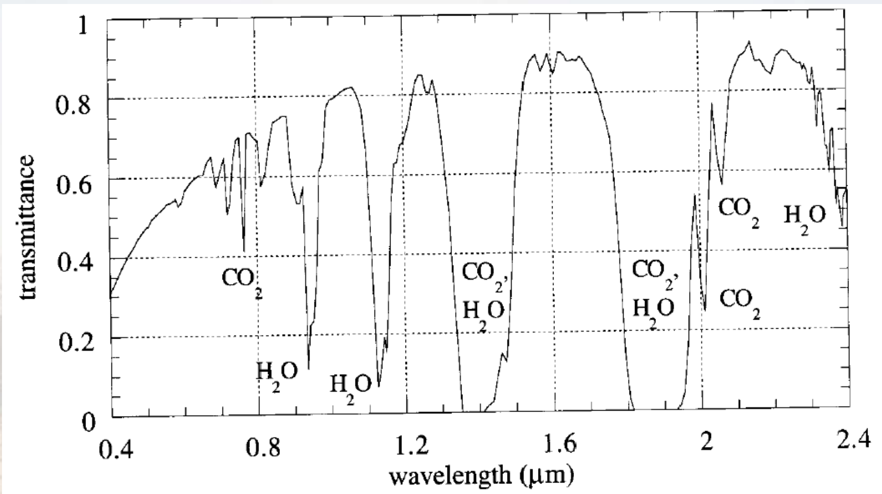

- The molecular absorption bands of water and carbon dioxide cause deep absorption features
- Near 1.4 and 1.9 μm bands, completely block transmission of radiation

Terrain reflection

Incident irradiance modified to account for terrain shape:

$$E_\lambda(x,y) = \tau_s(\lambda)E_\lambda^0\, \hat{\mathbf{n}}(x,y) \bullet \hat{\mathbf{s}}$$
$$= \tau_s(\lambda)E_\lambda^0 \cos\left[\theta(\mathrm{x},\mathrm{y})\right]$$

Where

$\hat{\mathbf{n}}(x,y)$

= The outside normal vector of the surface

$\hat{\mathbf{s}}$ = Negative vector of the incident flux density

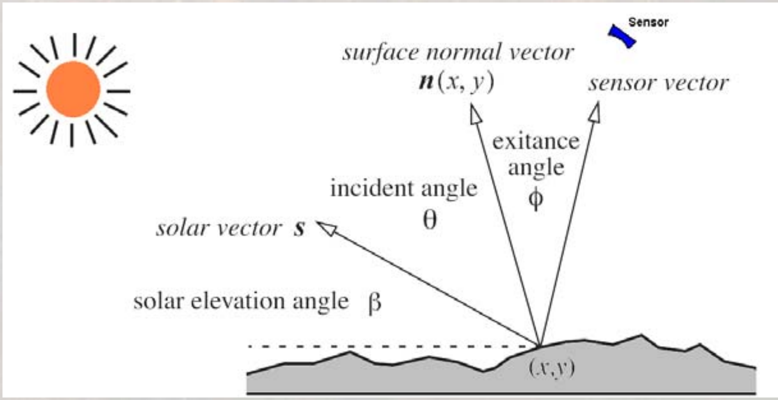

Radiance leaving from the (Lambertian) surface :

$$L_\lambda(x,y) = \rho(x,y,\lambda)\frac{E_\lambda(x,y)}{\pi}$$
$$= \rho(x,y,\lambda)\frac{\tau_s(\lambda)E_\lambda^0}{\pi}\cos\left[\theta(\mathrm{x},\mathrm{y})\right]$$

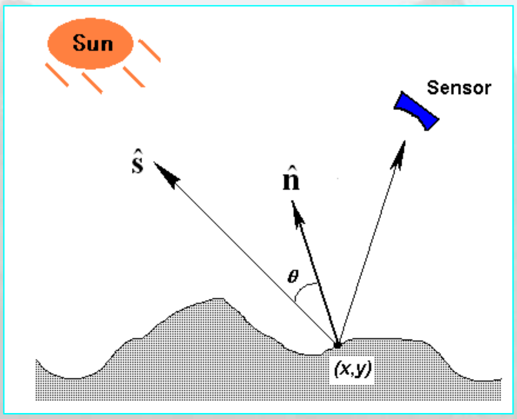

where

$\rho(x,y,\lambda)$

=diffuse spectral reflectance

Note: for *Lambertian surface*, $\rho(x,y,\lambda)$ is a function of the position as well as the wavelength, but not that of the viewing direction of the sensor!

$$L_\lambda(x,y) = \rho(x,y,\lambda)\frac{E_\lambda(x,y)}{\pi}$$
$$= \rho(x,y,\lambda)\frac{\tau_s(\lambda)E_\lambda^0}{\pi}\cos[\theta(\mathrm{x},\mathrm{y})]$$

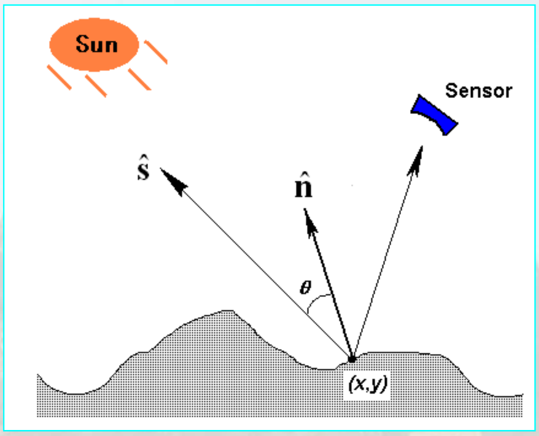

If the surface is **NOT Lambertian**, then $\frac{\rho(x,y,\lambda)}{\pi}$ must be replaced by a different function called

Bi-directional Reflectance Distribution Function (BRDF)

which is a function of incident and viewing angles, as well as wavelength

BRDF Model

BRDF is dependent on

- Angles between the Sun, the Earth surface, and the sensor;
- The surface shape;
- The types of surface materials (which in turn determine the types of reflections such as specular, diffusion).

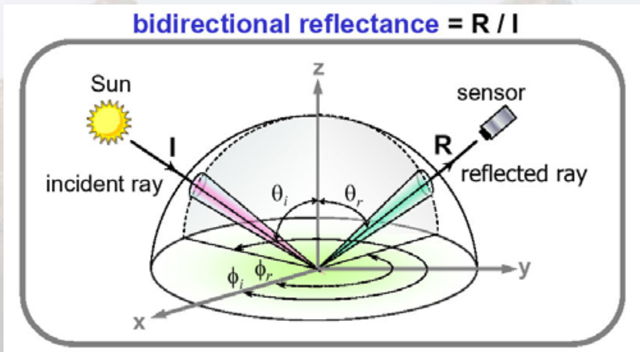

$$\rho(\theta_i,\varphi,\theta_r,\varphi_r) = \rho_d[(1-\beta)\cdot\delta(\theta_i,\theta_r)\cdot\delta(\varphi_i,\varphi_r \pm \pi) + \frac{\beta}{\pi}]$$

BRDF — Specular reflection — diffusion

Considering the transmittance between surface and the Sensor (upward):

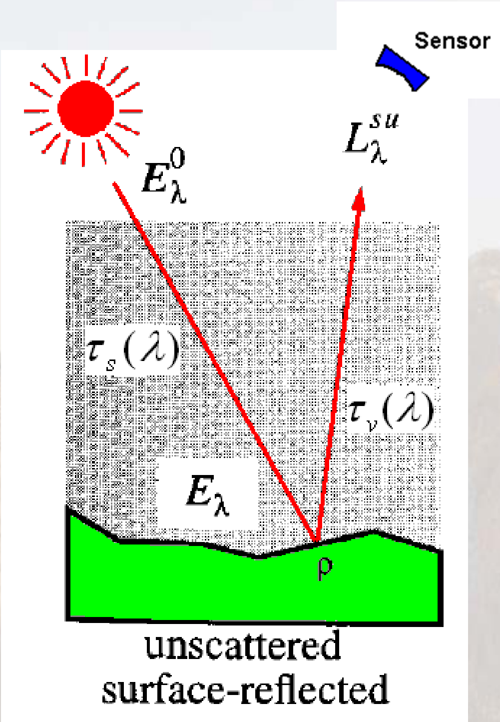

$$L_\lambda^{su} = \tau_v(\lambda) L_\lambda$$

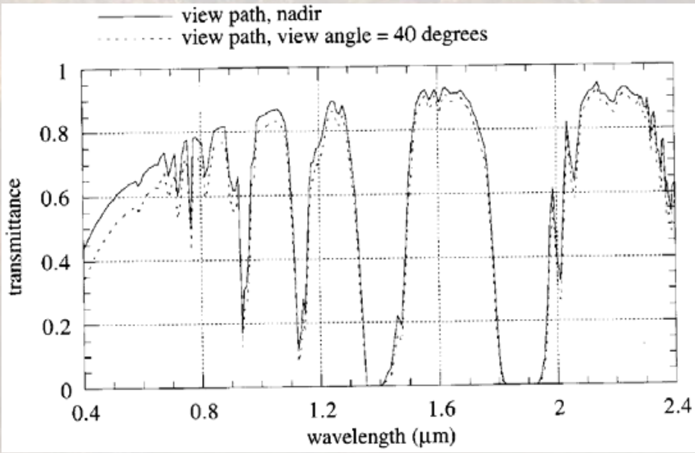

Lastly, At the Sensor, **incident irradiance** from the surface-reflected solar radiation is

$$L_\lambda^{su}(x,y,\lambda) = \tau_v(\lambda) L_\lambda(x,y,\lambda)$$
$$= \rho(x,y,\lambda) \frac{\tau_v(\lambda)\tau_s(\lambda)E_\lambda^0}{\pi} \cos[\theta(x,y)]$$

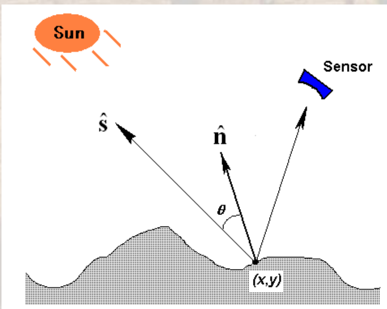

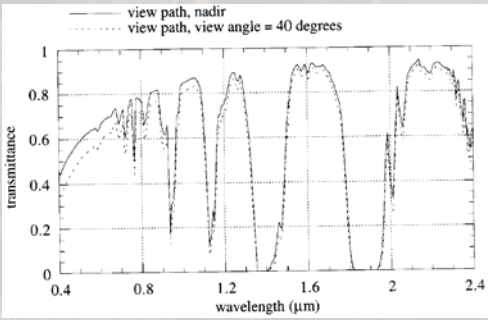

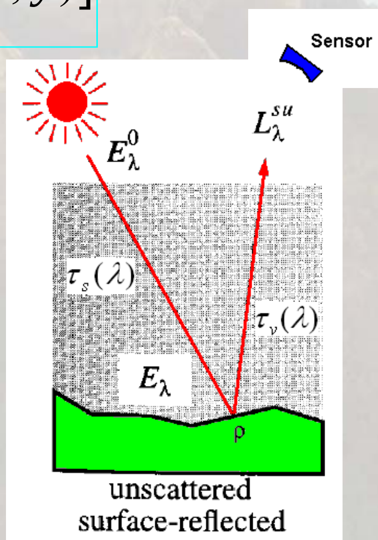

The down-scattered, surface-reflected skylight

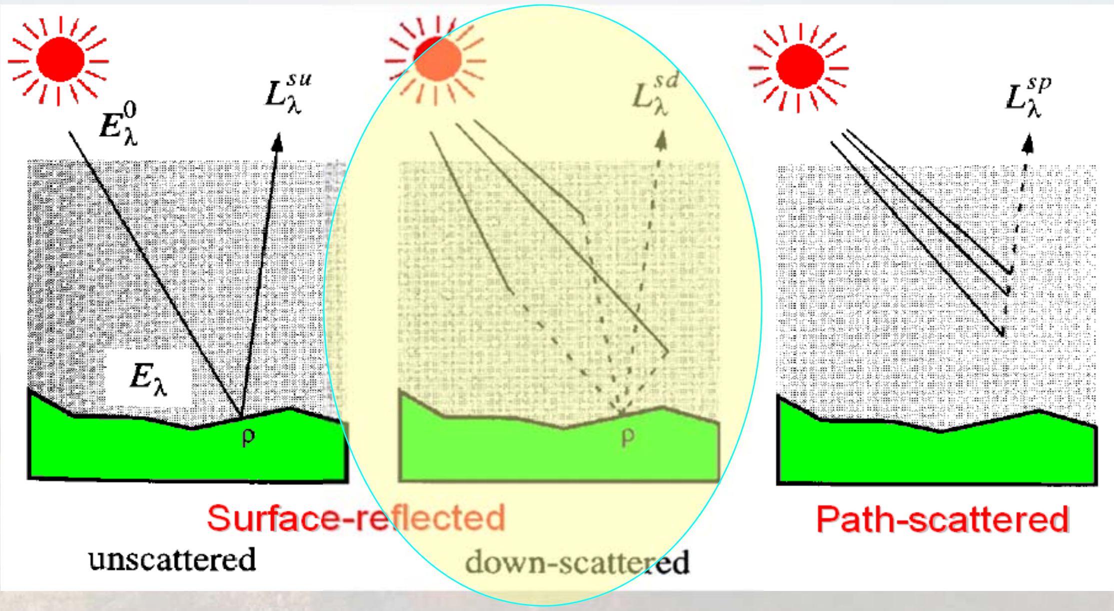

- The unscattered, surface-reflected radiation
- The down-scattered, surface-reflected skylight
- The up-scattered path radiance

$$L_\lambda^s = L_\lambda^{su} + L_\lambda^{sd} + L_\lambda^{sp}$$

The down-scattered, surface-reflected skylight

Atmosphere-Scattered downward (skylight) , and then surface-reflected upward:

$$L_\lambda^{sd}$$

$$L_\lambda^s = L_\lambda^{su} + L_\lambda^{sd} + L_\lambda^{sp}$$

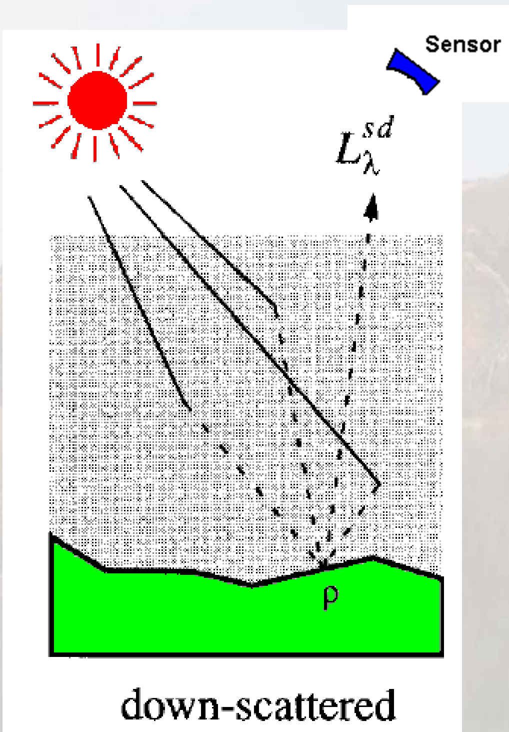

$$L_\lambda^{sd} = F(x,y,\lambda)\rho(x,y,\lambda)\frac{\tau_v(\lambda)E_\lambda^d}{\pi}$$

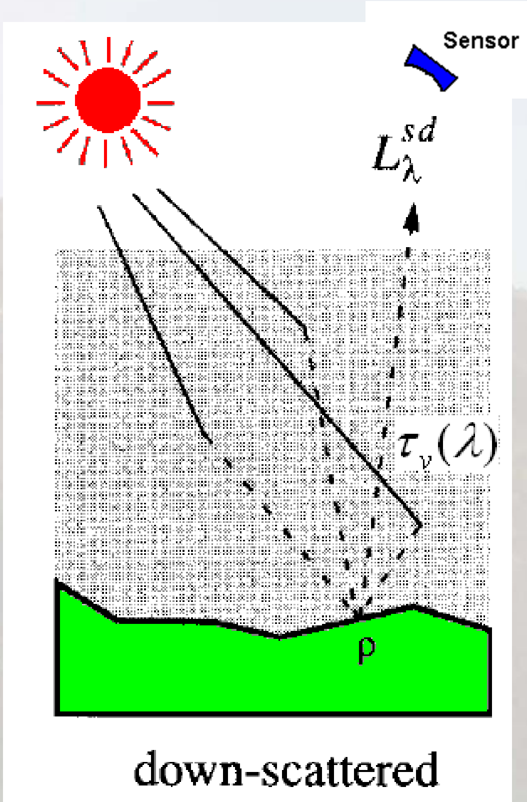

where

E_λ^d = irradiance due to skylight at the surface, which is directly measurable by instruments at the ground

$F(x,y,\lambda)$

= a factor related to the intervening topography between the pixel and the sky, which accommodates the possibility that the sky might not be entirely visible from the pixel of interest due to topography intervening.

Lastly, At the Sensor, **incident irradiance** from surface-reflected skylight radiation is

$$L_\lambda^{sd} = F(x,y,\lambda)\rho(x,y,\lambda)\frac{\tau_v(\lambda)E_\lambda^d}{\pi}$$

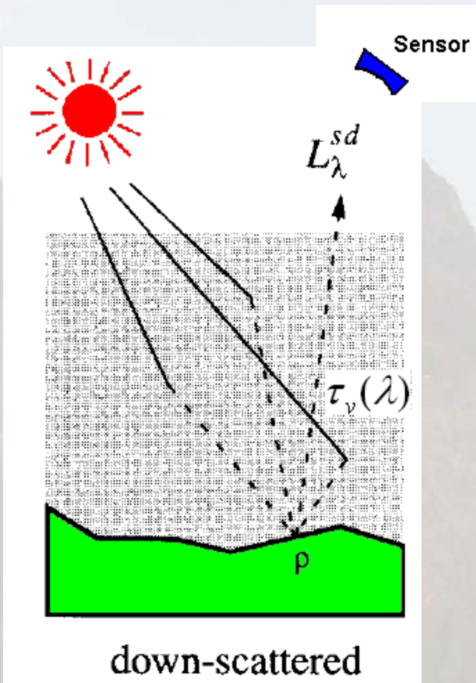

This term is responsible for the commonly observed fact that shadows in the images are not totally dark.

The up-scattered path radiance

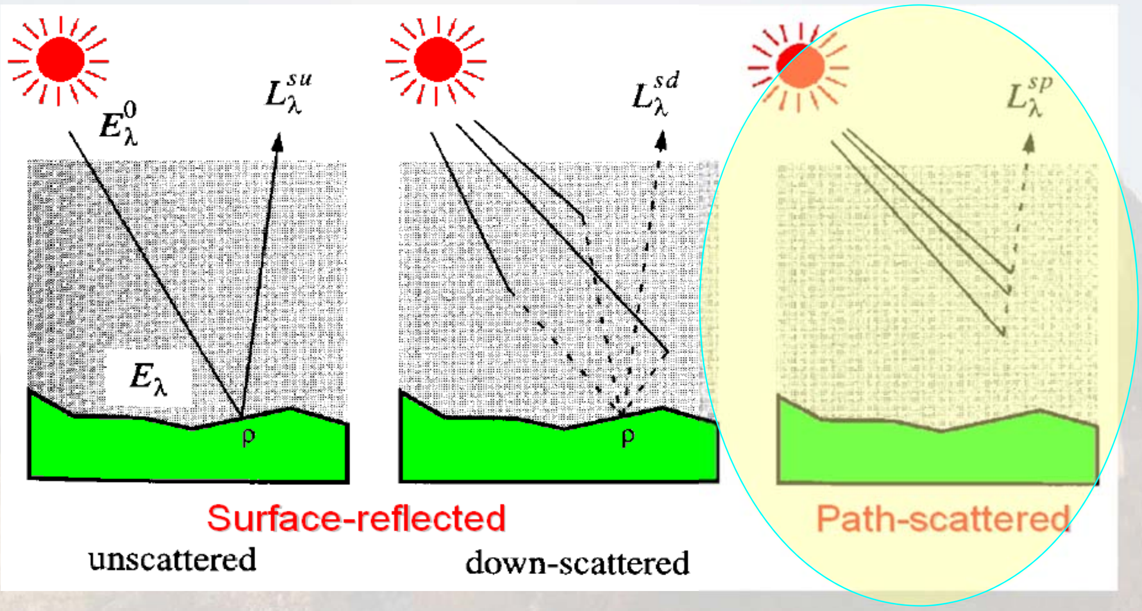

- The unscattered, surface-reflected radiation
- The down-scattered, surface-reflected skylight
- The up-scattered path radiance

$$L_\lambda^s = L_\lambda^{su} + L_\lambda^{sd} + L_\lambda^{sp}$$

The up-scattered path radiance

$$L_\lambda^{sp}$$

$$L_\lambda^s = L_\lambda^{su} + L_\lambda^{sd} + L_\lambda^{sp}$$

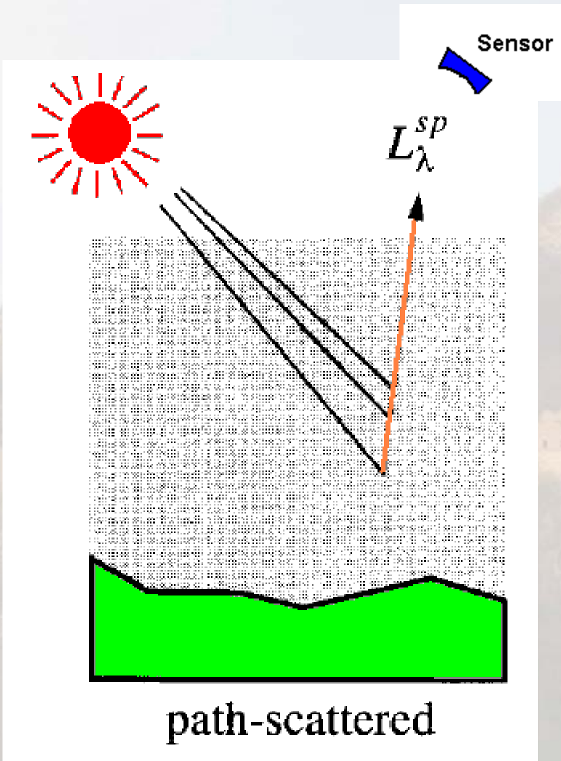

Path-Scattered upward Component:

$$\boxed{L_\lambda^{sp} = L_\lambda^{Rayleigh} + L_\lambda^{Mie}}$$

Molecule: $L_\lambda^{Rayleigh} \propto \lambda^{-4}$

Aerosol: L_λ^{Mie}

$$L_\lambda^{sp} \propto \lambda^{-2} \sim \lambda^{-0.7}$$

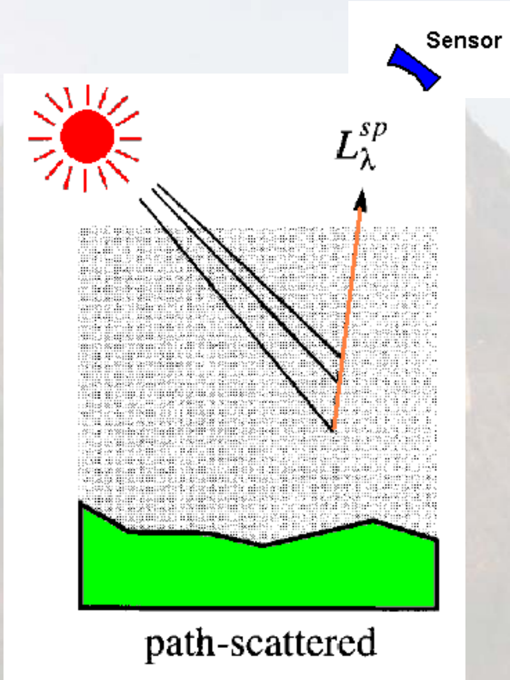

$$\boxed{L_\lambda^{sp} = L_\lambda^{Rayleigh} + L_\lambda^{Mie}}$$

Path radiance

- Varies within a scene (such as a rural and an urban area, smoke plume impact, and so on)
- Varies with view angles

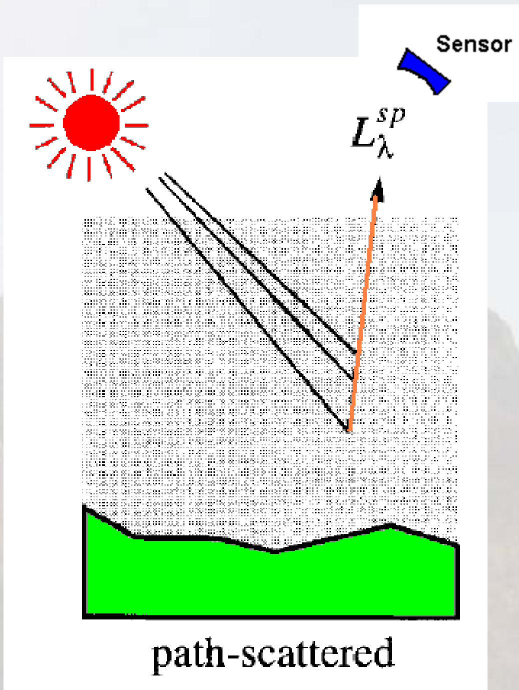

As a consequence, the path-scattered components might be quite different across the FOV for a wide FOV sensor !

Total at-sensor Radiance

$$L_\lambda^s(x,y) = L_\lambda^{su}(x,y) + L_\lambda^{sd}(x,y) + L_\lambda^{sp}(x,y)$$

$$L_\lambda^{su} = \rho(x,y,\lambda)\frac{\tau_v(\lambda)\tau_s(\lambda)E_\lambda^0}{\pi}\cos[\theta(x,y)]$$

$$L_\lambda^{sd} = F(x,y,\lambda)\rho(x,y,\lambda)\frac{\tau_v(\lambda)E_\lambda^d}{\pi}$$

$$L_\lambda^{sp} = L_\lambda^{Rayleigh} + L_\lambda^{Mie}$$

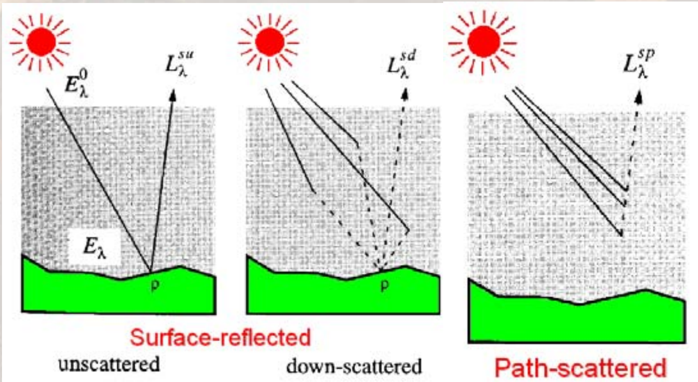

Total at-sensor Radiance

$$\begin{aligned} L_\lambda^s(x,y) &= L_\lambda^{su}(x,y) + L_\lambda^{sd}(x,y) + L_\lambda^{sp}(x,y) \\ &= \rho(x,y,\lambda)\frac{\tau_v(\lambda)}{\pi}\{\tau_s(\lambda)E_\lambda^0\cos[\theta(x,y)] + F(x,y,\lambda)E_\lambda^d\} + L_\lambda^{sp}(x,y) \end{aligned}$$

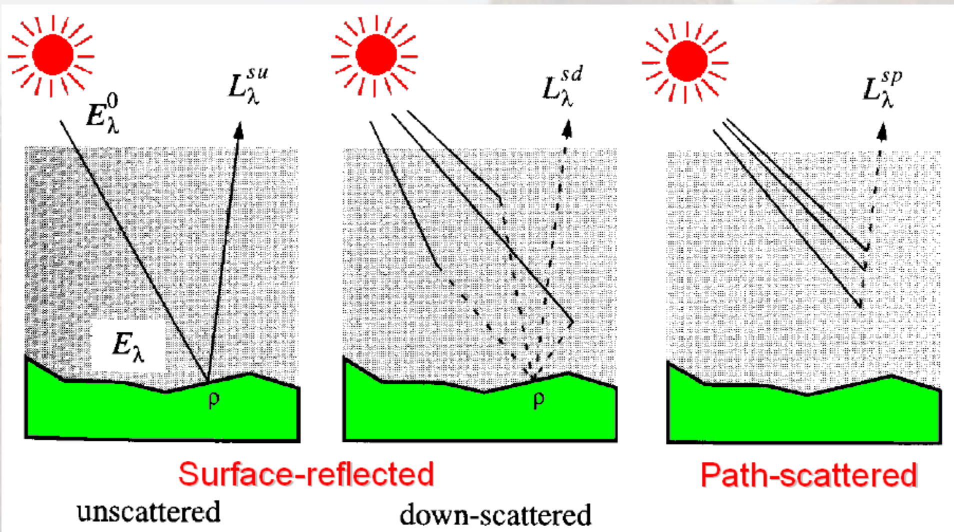

Total at-sensor Radiance

$$L_\lambda^s(x,y) = L_\lambda^{su}(x,y) + L_\lambda^{sd}(x,y) + L_\lambda^{sp}(x,y)$$
$$= \rho(x,y,\lambda)\frac{\tau_v(\lambda)}{\pi}\{\tau_s(\lambda)E_\lambda^0\cos[\theta(x,y)] + F(x,y,\lambda)E_\lambda^d\} + L_\lambda^{sp}(x,y)$$

- The total spectral radiance received by the sensor is **linearly proportional to the surface diffuse reflectance** (or BRDF), modified by
- **A multiplicative**, spatially- and spectrally-variant **factor** that depends on the terrain shape, and
- **An additive**, spatially-invariant, spectrally-dependent **term** due to viewing path scattering

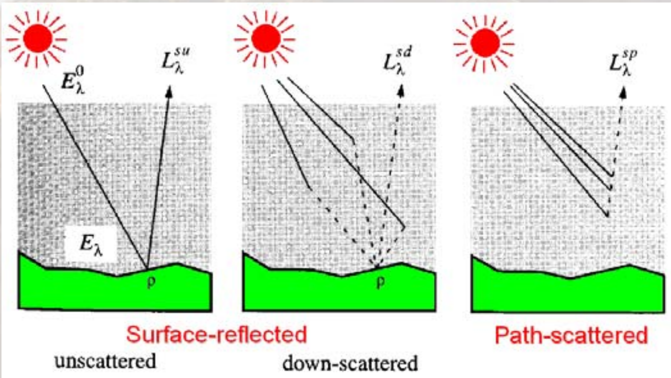

Some examples:

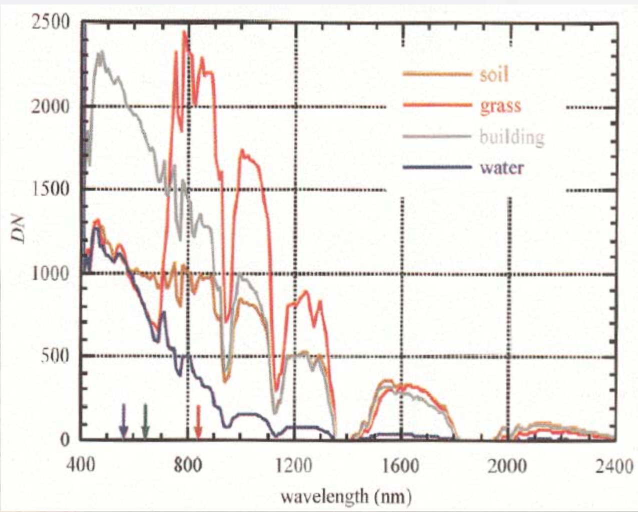

AVIRIS image of Palo Alto, CA, illustrating hyperspectral data

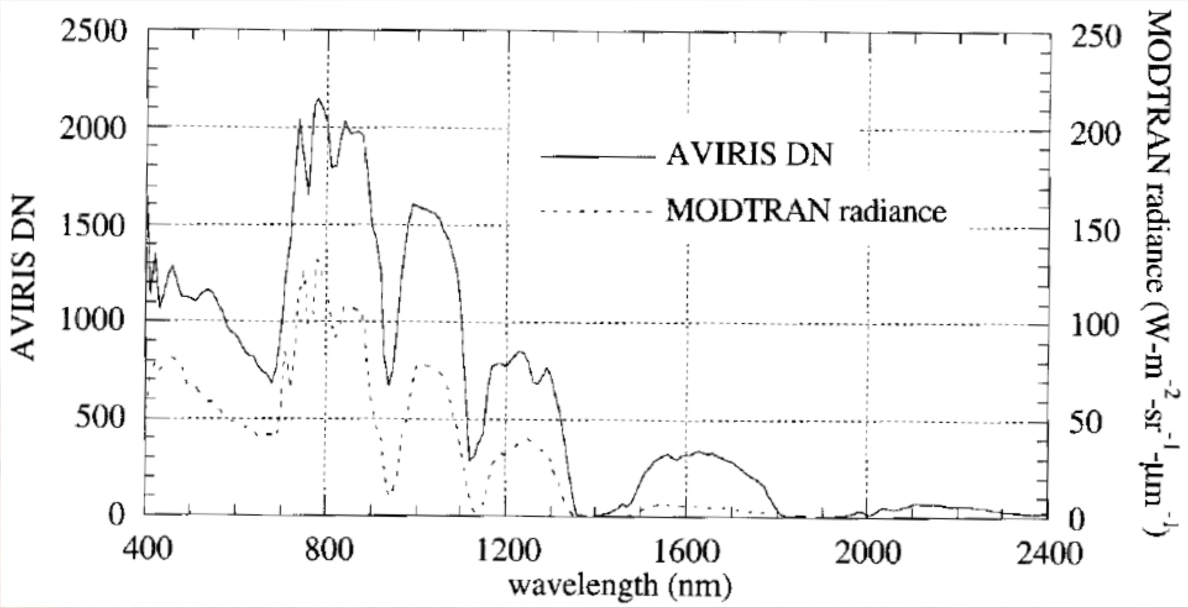

Kentucky Bluegrass, MODTRAN predicted and plot of a mixed grass & trees from the AVIRIS image of Palo Alto, CA

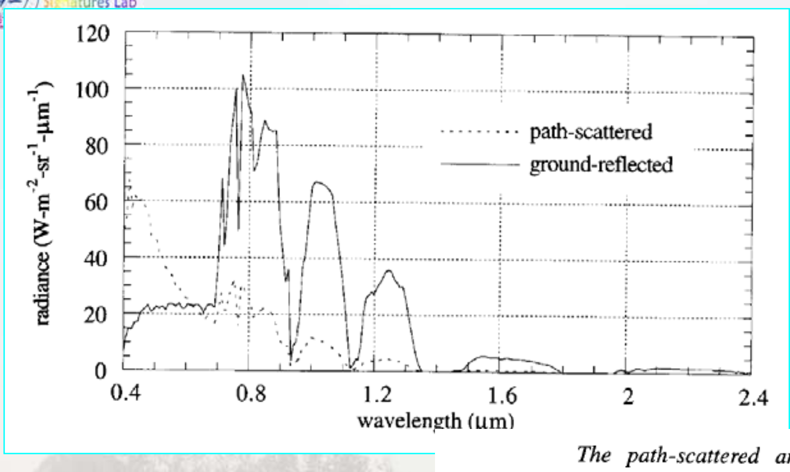

Path-scattered vs. Ground-reflected

Spectral radiance of the Kentucky Bluegrass

The path-scattered and ground-reflected components of the total upwelling radiance seen by a satellite sensor for a surface reflectance of Kentucky Bluegrass. These components, as defined in MODTRAN, are related to the terms of Eq. (2 – 10) as follows. The path-scattered component is L_λ^{sp}, plus radiation that is reflected by the surface in a direction other than towards the sensor (remember, we assume the surface is perfectly diffuse and reflects equally in all directions), and is then scattered into the IFOV (we have not included this term in our discussion). The strong increase in the path-scattered component below 0.7µm is due to molecular scattering and is primarily the L_λ^{sp} term, since the surface reflectance here is relatively low. Above 0.7µm, the influence of the reflected and then scattered component is apparent. The ground-reflected component is the sum of L_λ^{su} and L_λ^{sd}. In the ground-reflected component, little information about the grass signature is seen until above 0.7µm, where the reflectance becomes relatively high. The ground-reflected component only exceeds the path-scattered component above 0.7µm, but both contain information about the signal (grass reflectance). Note the atmospheric water vapor absorption bands near 0.9, 1.1, 1.4 and 1.9µm.

Spectral reflectance vs. at-sensor radiance

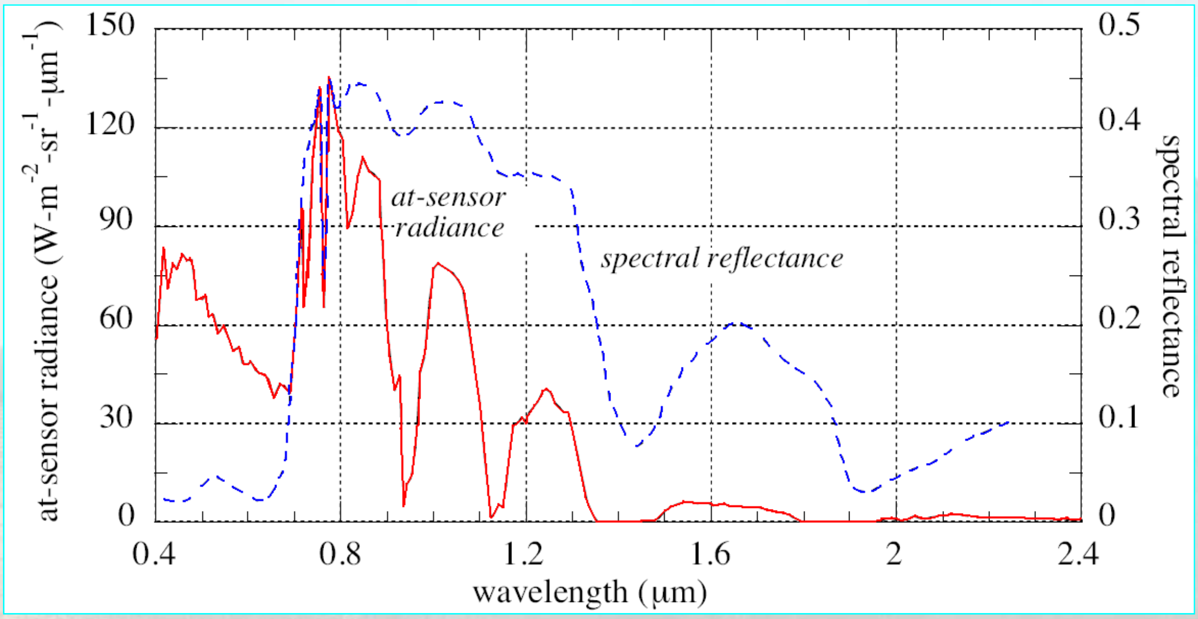

注意：传感器口面的辐射量同被感知物质（肯塔基草）的光谱反射率之间的巨大差异 --- 因此，既要研究物质的光谱特性，也要研究传输特性，还要研究传感器特性，同时考虑图像处理算法的影响！

$$L_\lambda^s(x,y) = \rho(x,y,\lambda)\frac{\tau_v(\lambda)}{\pi}\{\tau_s(\lambda)E_\lambda^0\cos[\theta(x,y)] + F(x,y,\lambda)E_\lambda^d\} + L_\lambda^{sp}(x,y)$$

Terrain Shading Factors

Upper left: Digital Elevation Model (DEM) with GSI of 30 m

Upper right: Shaded relief image calculated from DEM by $\cos[\theta(x,y)]$

Lower: Thematic mapper (TM) image (left) and contrast-stretched TM image (right)

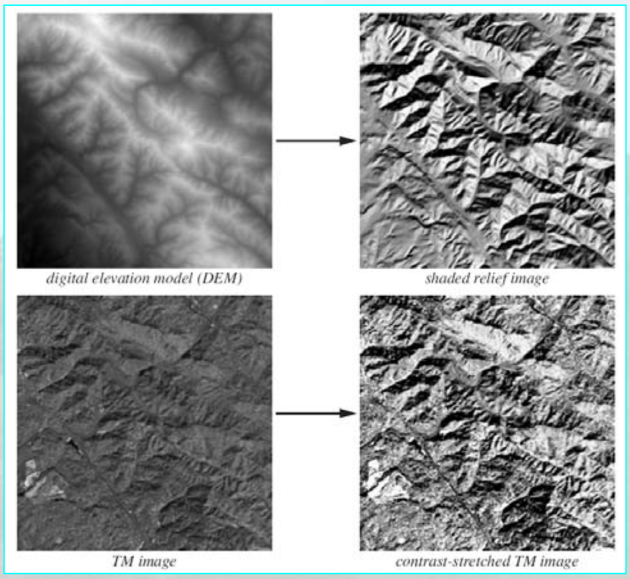

The similarity between the shaded relief image and the contrast-stretched TM image is **evident**.

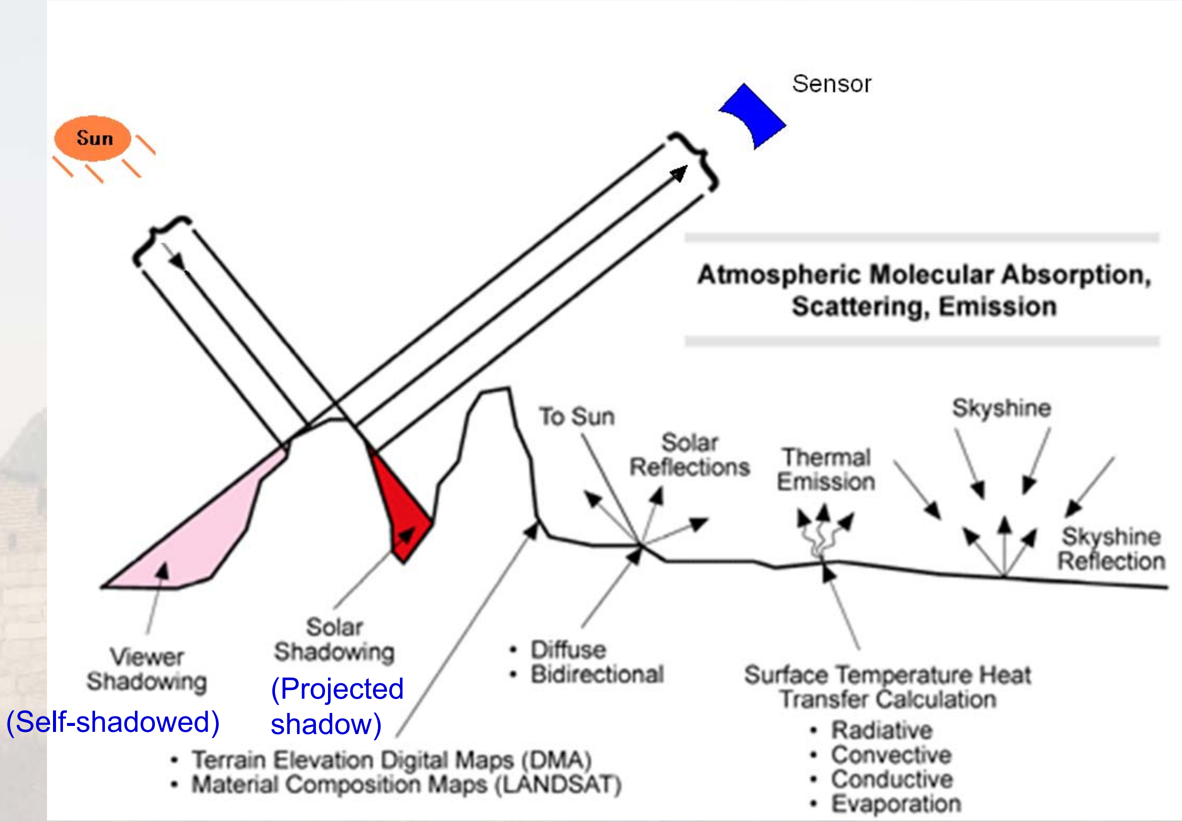

Shadowing

Upper left: Shaded relief image calculated from DEM

Upper right: Contrast-stretched TM image

Lower: Self-shadowed pixels (left) and pixels of projected shadows (right)

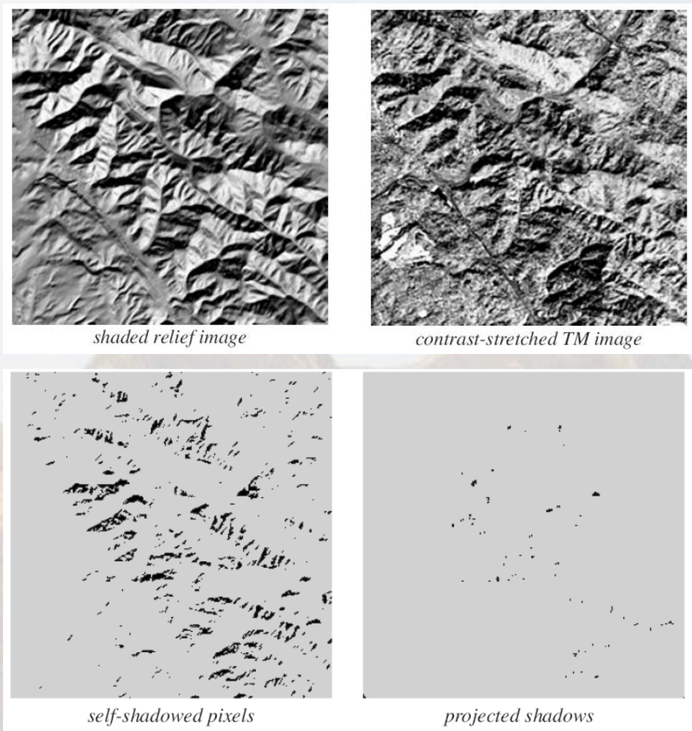
shaded relief image | contrast-stretched TM image
self-shadowed pixels | projected shadows

For the current image, the projected shadows are relatively fewer due to the fact of mild terrain relief and high solar elevation for TM images.

Sun Shadows

Sun elevation 65 deg. | Sun elevation 38 deg.

Less projected shadowing

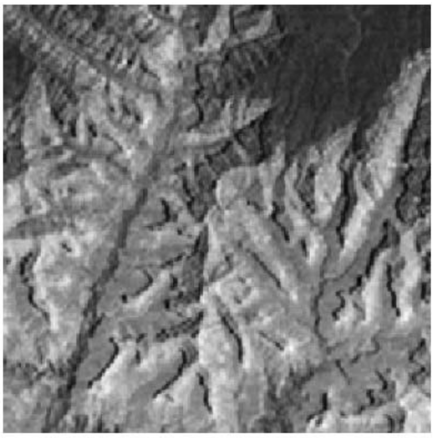

June 11, 1981

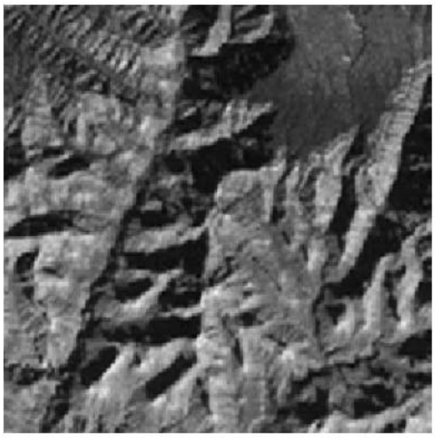

October 20, 1980

More projected shadowing

Landsat MSS images of the Grand Canyon, Arizona, acquired on two dates. The lower sun elevation of 38° for the October image dramatically increases the shadowing in the Canyon, compared to the June image with a sun elevation of 65°.

Dark object used for atmosphere Correction

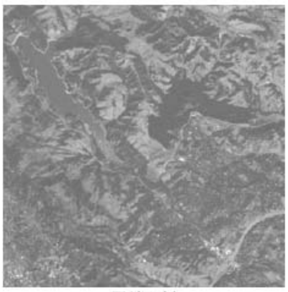

TM band 1

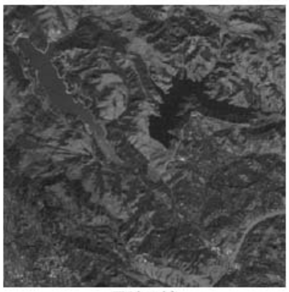

TM band 2

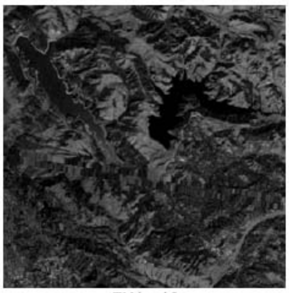

TM band 3

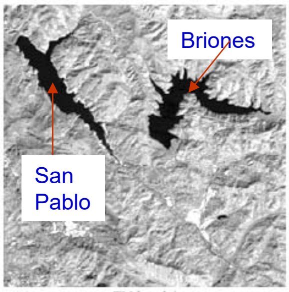

TM band 4

TM band 1 through band 4 images of the San Pablo (left) and Briones Reservoirs (right) north of Berkeley, California (part of the same TM scene used in Fig. 2-11). The individual bands are uncalibrated and shown with their recorded relative brightness and contrast. Atmospheric scattering reduces the contrast in band 1, while bands 2 and 3 are dark, due to low vegetation reflectance and lower sensor gain than band 1. Band 4 shows high contrast between the water-filled reservoirs and surrounding vegetated and bare soil terrain. Note the Briones Reservoir is relatively darker in the shorter wavelength spectral bands than the San Pablo Reservoir. This indicates the latter may have suspended sediments and particulates in the water, which is particularly likely since it is at a lower altitude and subjected to more runoff from the surrounding terrain. In band 4, both reservoirs have little radiance because of the near zero reflectance of water in the NIR.

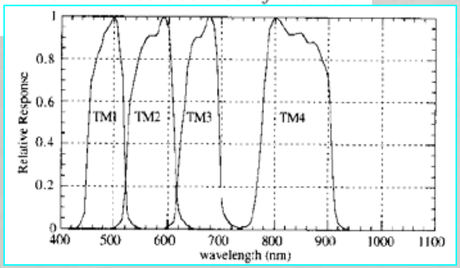

第四讲 红外辐射模型

(Infrared Radiation Models)

- VNIR和SWIR谱段辐射模型
- MWIR和TIR谱段辐射模型
- 红外辐射模型的拓展：空中目标的红外辐射建模

MWIR＆TIR谱段传感器所感兴趣的物理量—温度、光谱反射率

name	wavelength range	radiation source	surface property of interest
Visible (V)	0.4 – 0.7μm	solar	reflectance
Near InfraRed (NIR)	0.7 – 1.1μm	solar	reflectance
Short Wave InfraRed (SWIR)	1.1 – 1.35μm 1.4 – 1.8μm 2 – 2.5μm	solar	reflectance
Mid Wave InfraRed (MWIR)	3 – 4μm 4.5 – 5μm	solar, thermal	reflectance, temperature
Thermal InfraRed (TIR)	8 – 9.5μm 10 – 14μm	thermal	temperature
microwave, radar	1mm – 1m	thermal (passive) artificial (active)	temperature (passive) roughness (active)

General Cases

From MWIR to TIR:

- Solar irradiance
- Self-emitted thermal radiation from a Lambertian object

For TIR: direct solar radiation is ignorable except for special surfaces where

- Solar-induced heating of the surface is essential; and/or
- Specular reflection from the surface is dominant.

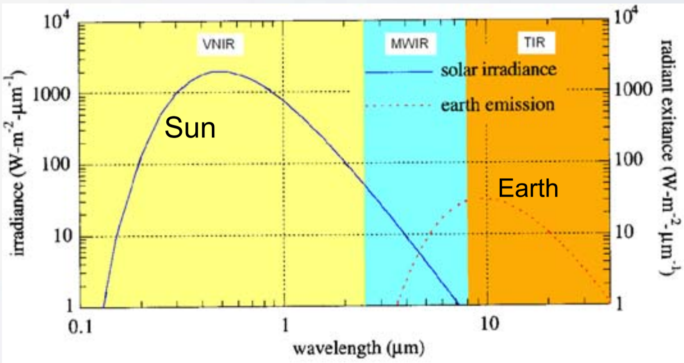

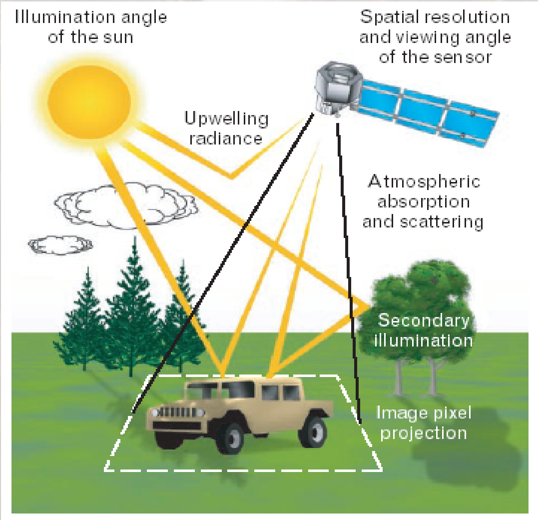

Solar Irradiance in the MWIR & TIR Regions

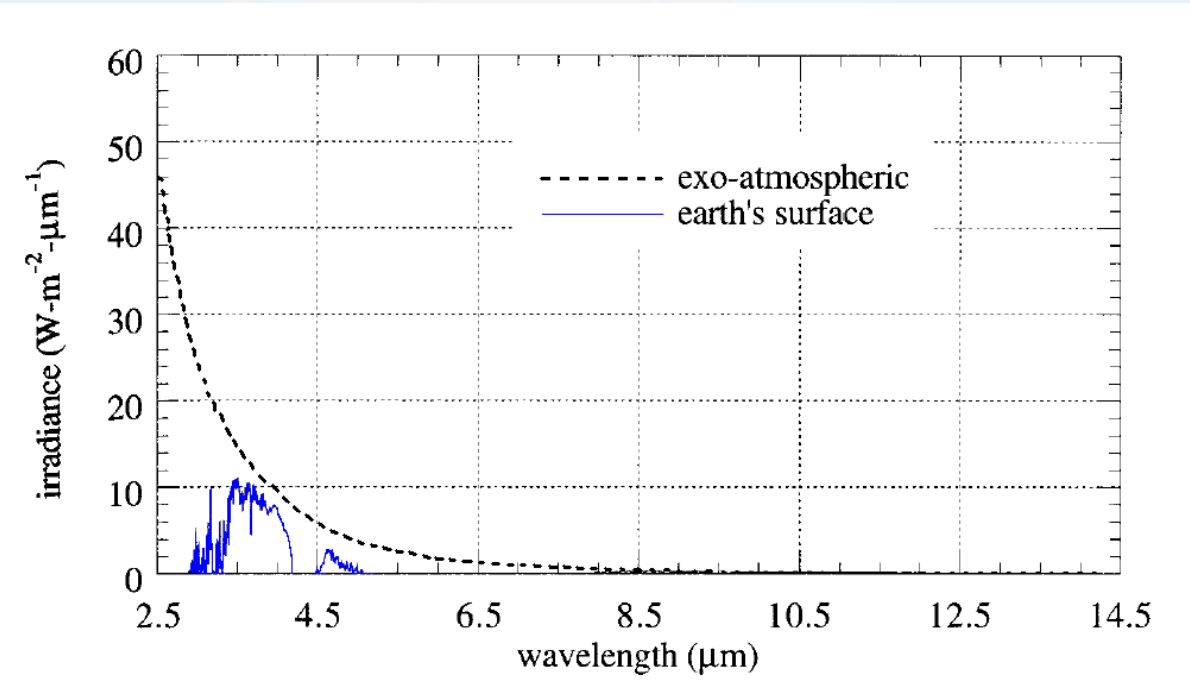

Radiation Components

In the MWIR region:

$$L_\lambda^{MWIR} = L_\lambda^s + L_\lambda^e$$

In the TIR region:

$$L_\lambda^{TIR} = L_\lambda^e$$

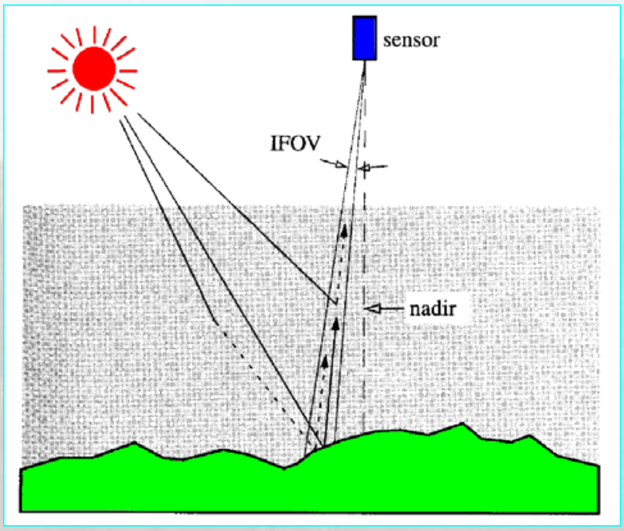

where

L_λ^s = Solar related, as discussed before

L_λ^e =total at-sensor radiance from emission, as will be discussed below

Reflected and scattered (Solar-related) components:

$$L_\lambda^s = \sum$$

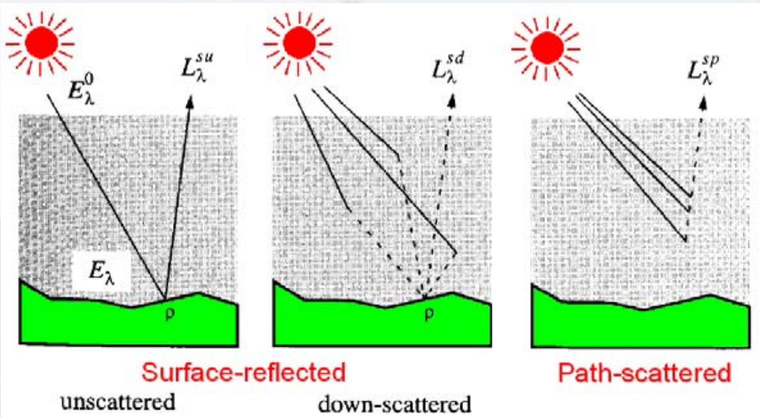

(a) reflected and scattered components

Emitted components:

$$L_\lambda^e = \sum$$

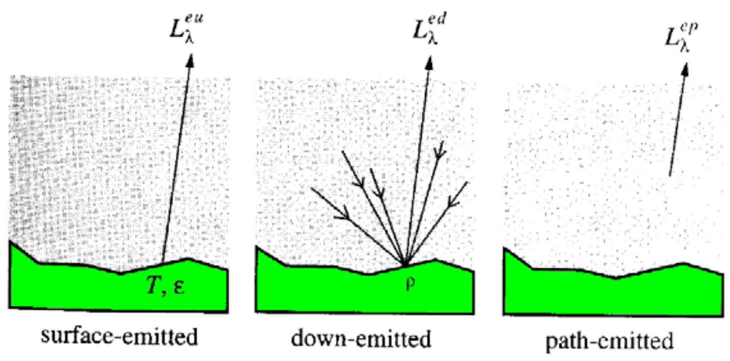

(b) emitted components

L_λ^{eu} = the surface-emitted radiation from the earth

L_λ^{ed} = the down-emitted, surface-reflected radiation from the atmosphere

L_λ^{ep} = the path-emitted radiance

Surface-Emitted Component

The emitted radiance at Earth's surface:

$$L_\lambda(x,y) = \varepsilon(x,y,\lambda)\frac{M_\lambda[T(x,y)]}{\pi}$$

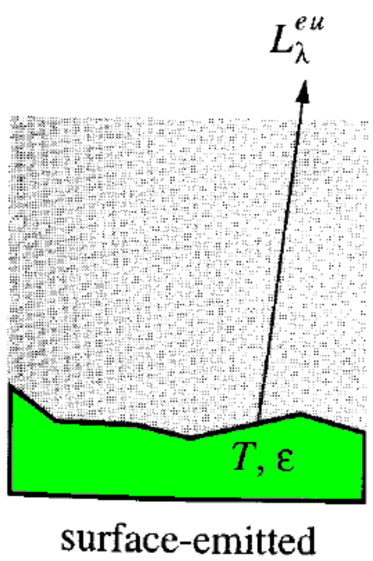

$$M_\lambda\left[T(x,y)\right]$$

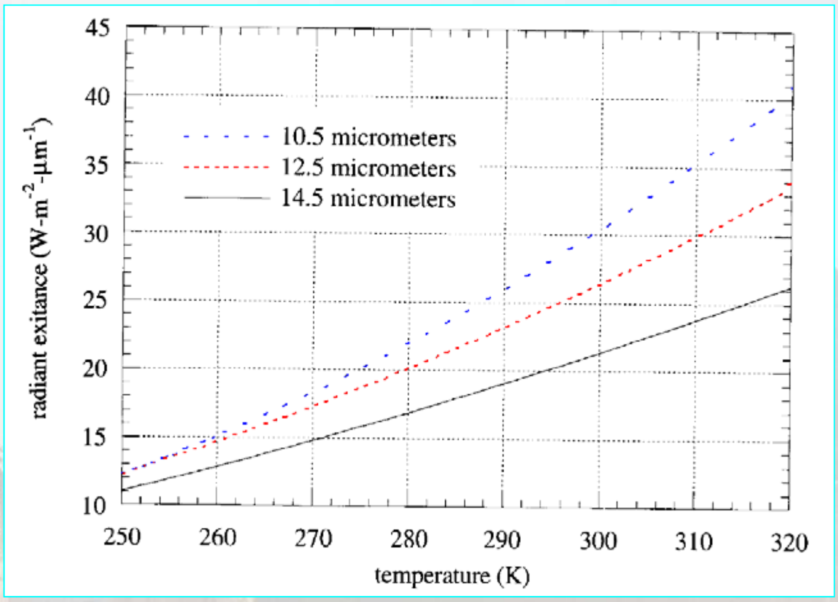

The dependence of radiant exitance from a blackbody on its temperature, at three wavelengths. Emissivity is held constant at one, whereas it actually can vary with temperature and wavelength for a greybody. The temperature range depicted is that for normal temperatures at the earth's surface.

Linear approximation

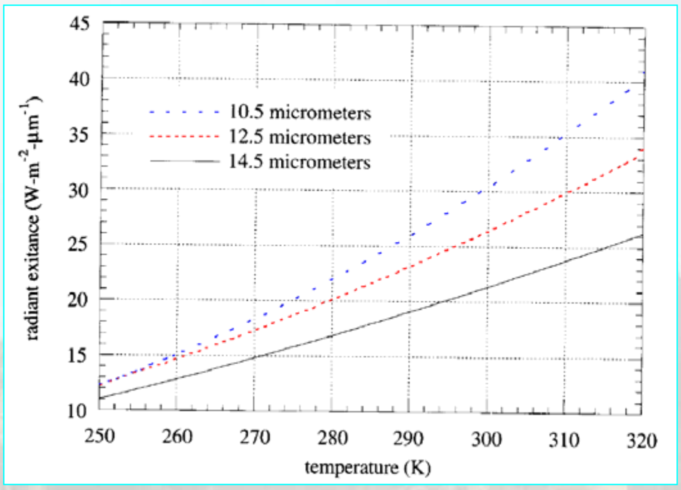

$$M_\lambda\left[T(x,y)\right] \approx a_\lambda T(x,y) + b_\lambda$$

$$L_\lambda(x,y) \approx \varepsilon(x,y,\lambda)\frac{[a_\lambda T(x,y) + b_\lambda]}{\pi}$$

Where a_λ and b_λ are relatively weak function of wavelength

Transmittance between surface and the sensor (upward):

$$\tau_v(\lambda)$$

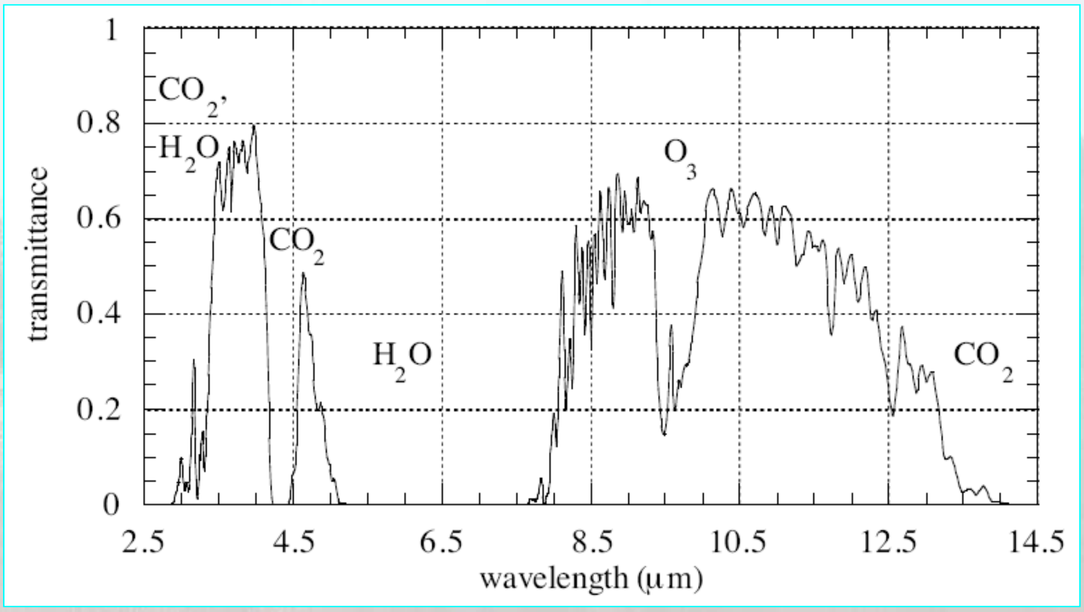

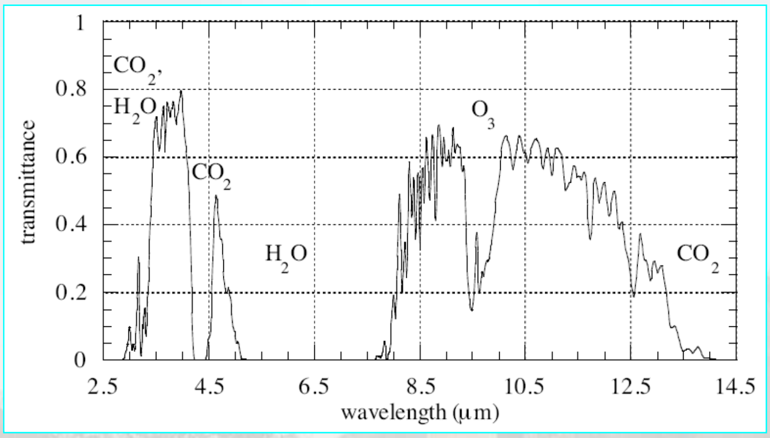

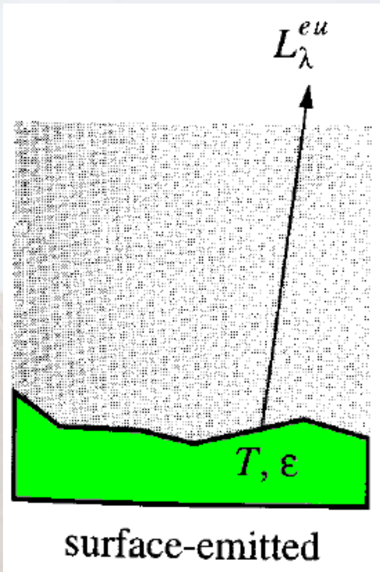

At-Sensor:

$$L_\lambda^{eu}(x,y) = \tau_v(\lambda) L_\lambda(x,y)$$
$$= \varepsilon(x,y,\lambda)\frac{\tau_v(\lambda) M_\lambda[T(x,y)]}{\pi}$$
$$\approx \varepsilon(x,y,\lambda)\frac{\tau_v(\lambda)[a_\lambda T(x,y) + b_\lambda]}{\pi}$$

Surface-Reflected, Atmosphere-Emitted Component

At-Sensor:

$$L_\lambda^{ed} = F(x,y,\lambda)\rho(x,y,\lambda)\frac{\tau_v(\lambda)M_\lambda^a}{\pi}$$

where

M_λ^a

= atmosphere-emitted radiance

$F(x,y,\lambda)$

= a factor related to the intervening topography between the pixel and the sky

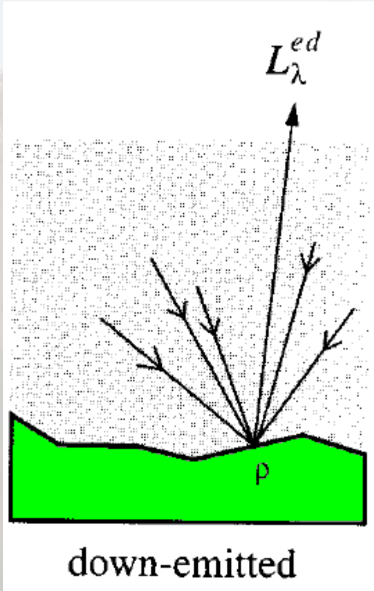

Kirchhoff's Law:

$$\rho(x,y,\lambda) = 1 - \varepsilon(x,y,\lambda)$$

$$L_\lambda^{ed} = F(x,y,\lambda)\rho(x,y,\lambda)\frac{\tau_v(\lambda)M_\lambda^a}{\pi}$$

$$= F(x,y,\lambda)[1-\varepsilon(x,y,\lambda)]\frac{\tau_v(\lambda)M_\lambda^a}{\pi}$$

Path-Emitted Component

L_λ^{ep} = the integration over the view path from the contribution of the atmospheric radiation as a function of temperature at different altitudes.

Extremely complicated !

However, it is reasonable to assume that this component does not vary significantly over a specified scene, except

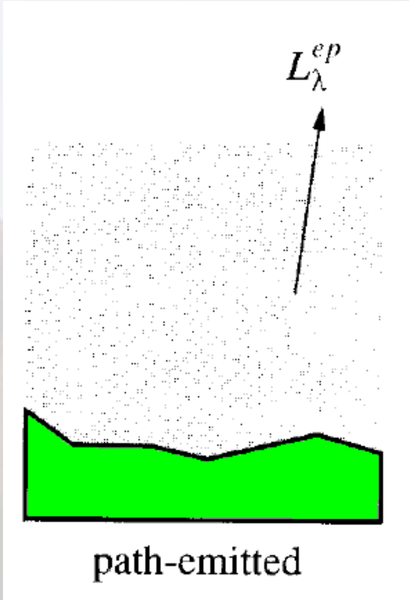

- For large angles from nadir (above about ±20 deg.), where the path-emitted term tends to increase, or
- In area where the surface temperature has significant spatial variation that may influence the near-surface atmospheric temperature.

Total at-Sensor Emitted Radiance

$$
\begin{aligned}
L_\lambda^{e}(x,y) &= L_\lambda^{eu}(x,y) + L_\lambda^{ed}(x,y) + L_\lambda^{ep}(x,y) \\
&= \varepsilon(x,y,\lambda)\frac{\tau_v(\lambda)}{\pi}\left[a_\lambda T(x,y)+b_\lambda\right] + F(x,y,\lambda)[1-\varepsilon(x,y,\lambda)]\frac{\tau_v(\lambda)M_\lambda^a}{\pi} + L_\lambda^{ep}(x,y) \\
&= \varepsilon(x,y,\lambda)\frac{\tau_v(\lambda)}{\pi}\left\{\left[a_\lambda T(x,y)+b_\lambda\right] - F(x,y,\lambda)M_\lambda^a\right\} + F(x,y,\lambda)\frac{\tau_v(\lambda)M_\lambda^a}{\pi} + L_\lambda^{ep}(x,y)
\end{aligned}
$$

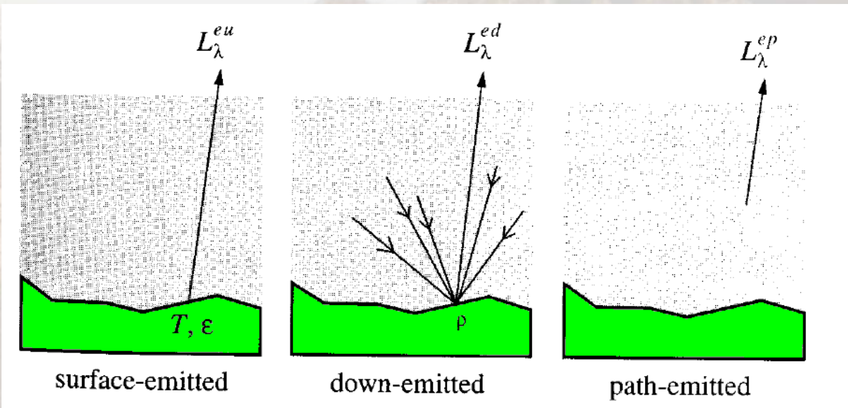

(b) emitted components

Total at-Sensor Emitted Radiance

$$L^{e}_{\lambda}(x,y) = \varepsilon(x,y,\lambda)\frac{\tau_v(\lambda)}{\pi}\left\{ \left[a_\lambda T(x,y) + b_\lambda\right] - F(x,y,\lambda)M^{a}_{\lambda} \right\} + F(x,y,\lambda)\frac{\tau_v(\lambda)M^{a}_{\lambda}}{\pi} + L^{ep}_{\lambda}(x,y)$$

- The total spectral radiance received by the sensor is approximately **linearly proportional to the surface temperature**, modified by
- **A multiplicative**, spatially- and spectrally-variant **emissivity factor**, and
- **An additive**, spatially-invariant, spectrally-dependent **term** due to viewing path emission

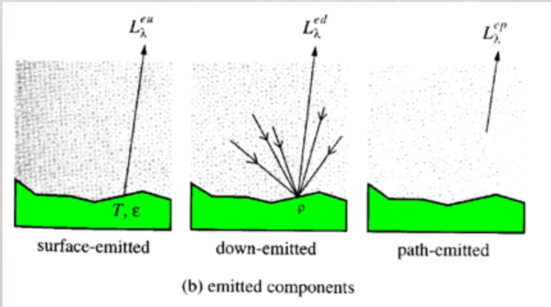

Total Solar and Thermal Upwelling Radiance

$$L_{\lambda}(x,y) = L^{s}_{\lambda}(x,y) + L^{e}_{\lambda}(x,y)$$

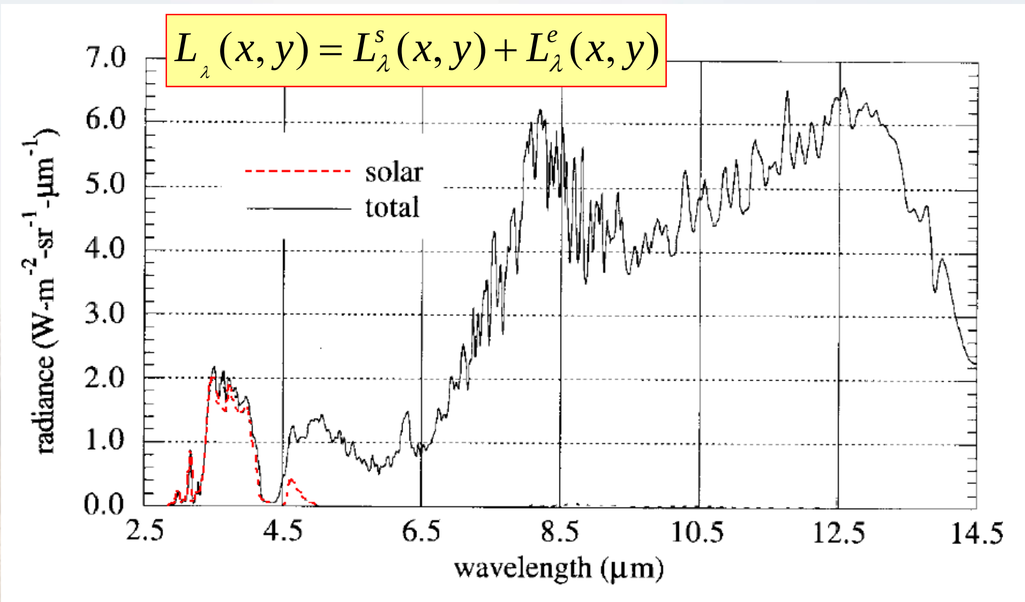

The at-sensor radiance above the atmosphere in the middle and thermal IR regions. Note how the two sources of radiation, solar and thermal emission, exchange relative importance from the MWIR to the TIR. The satellite view angle is zero degrees from nadir and the surface emissivity is assumed to be one. The spectral reflectance is also assumed to be uniform in wavelength.

Band-6:
10.4-12.5 μm

Clouds appear cooler than land in daytime TIR imagery

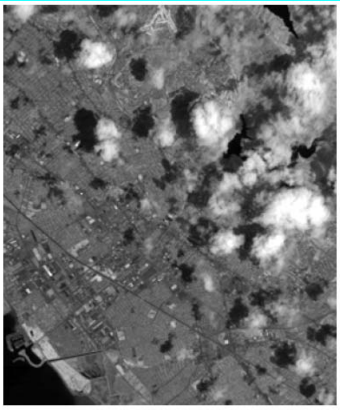

TM band 4

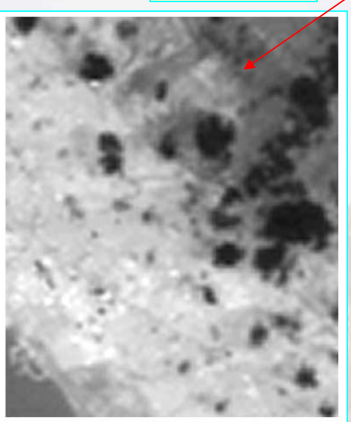

TM band 6

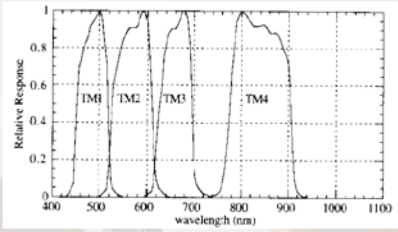

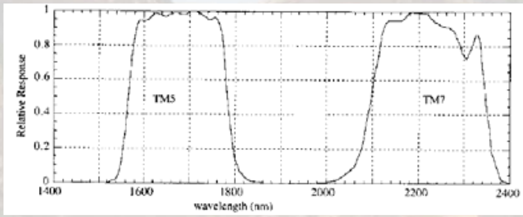

TM band 4 (30m GSI) and band 6 (120m GSI) images of the San Francisco area. The bright clouds visible in band 4 appear darker than the ground in band 6, implying they are cooler than the ground in this daytime image. The cloud shadows, visible to the upper left of each cloud in band 4, appear slightly darker than surrounding areas in band 6, implying that the ground in shadow is slightly cooler than that in sunlight. Note that weather satellite TIR images shown on television often have an inverted greyscale in order to make cold clouds appear bright!

"Heat Island" in Urban area

TM band 2

Visible

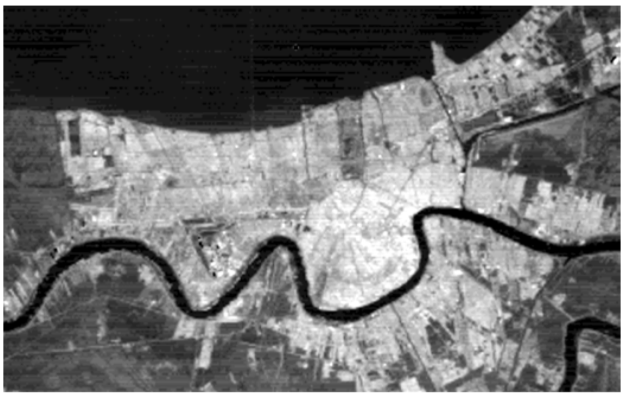

TM band 6

Thermal

Landsat TM band 2 and band 6 images of New Orleans, Louisiana, including Lake Pontchartrain and the Mississippi River (September 16, 1982). The urban area, particularly the denser core, appears warmer than surrounding vegetation, although their respective emissivities may be a factor. The darker, rectangular feature above the city center and adjoining the lake is a city park.

Thermal “Shadows”

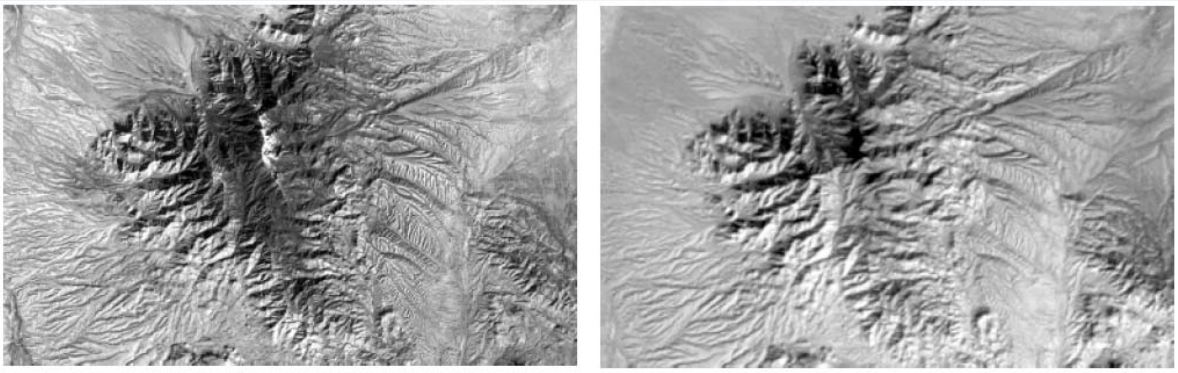

TM band 2 — Visible

TM band 6 — Thermal

Sunlight

The Santa Rita Mountains, south of Tucson, Arizona, viewed by Landsat TM on January 8, 1983. The elevation ranges from about 1000 meters to 2880 meters at Mt. Wrightson, and the mountains are heavily vegetated at the higher elevations. Note the thermal “shadows” on slopes facing away from the direction of solar irradiance (from the lower right); these valleys are cooler than the solar-facing slopes in this mid-morning, winter image.

Summary

VNIR $L^s_\lambda(x,y)$

MWIR $L_\lambda = L^s_\lambda + L^e_\lambda$

TIR $L^e_\lambda(x,y)$

name	wavelength range	radiation source	surface property of interest
Visible (V)	0.4 – 0.7µm	solar	reflectance
Near InfraRed (NIR)	0.7 – 1.1µm	solar	reflectance
Short Wave InfraRed (SWIR)	1.1 – 1.35µm 1.5 – 1.8µm 2 – 2.5µm	solar	reflectance
Mid Wave InfraRed (MWIR)	3 – 4µm 4.5 – 5µm	solar, thermal	reflectance, temperature
Thermal InfraRed (TIR)	8 – 9.5µm 10 – 14µm	thermal	temperature

Solar reflective components: $L^s_\lambda(x,y) = L^{su}_\lambda(x,y) + L^{sd}_\lambda(x,y) + L^{sp}_\lambda(x,y)$

Thermal emissive components: $L^e_\lambda(x,y) = L^{eu}_\lambda(x,y) + L^{ed}_\lambda(x,y) + L^{ep}_\lambda(x,y)$

Optical Radiation Model Summary

Solar reflective region:
VNIR

$$L_\lambda^s(x,y) = L_\lambda^{su}(x,y) + L_\lambda^{sd}(x,y) + L_\lambda^{sp}(x,y)$$
$$= \rho(x,y,\lambda)\frac{\tau_v(\lambda)}{\pi}\{\tau_s(\lambda)E_\lambda^0\cos[\theta(x,y)] + F(x,y,\lambda)E_\lambda^d\} + L_\lambda^{sp}(x,y)$$

MWIR +

Thermal region:
TIR

$$L_\lambda^e(x,y) = L_\lambda^{eu}(x,y) + L_\lambda^{ed}(x,y) + L_\lambda^{ep}(x,y)$$
$$= \varepsilon(x,y,\lambda)\frac{\tau_v(\lambda)}{\pi}\{[a_\lambda T(x,y) + b_\lambda] - F(x,y,\lambda)M_\lambda^a\}$$
$$+ F(x,y,\lambda)\frac{\tau_v(\lambda)M_\lambda^a}{\pi} + L_\lambda^{ep}(x,y)$$

- The sensor-collected energy is **proportional to** the surface reflectance (solar reflective region) and to the surface emissivity and temperature (thermal region);
- A **spatially-invariant**, but spectrally-dependent constant **bias term** arising from atmospheric scattering (solar reflective) and atmospheric emission (thermal region) is present in the sensed signature;
- A **coupling** exists between the surface and the atmosphere; they interact as a function of the surface reflectance, emission and topography.

More things must be done for this scene to be modeled, however …

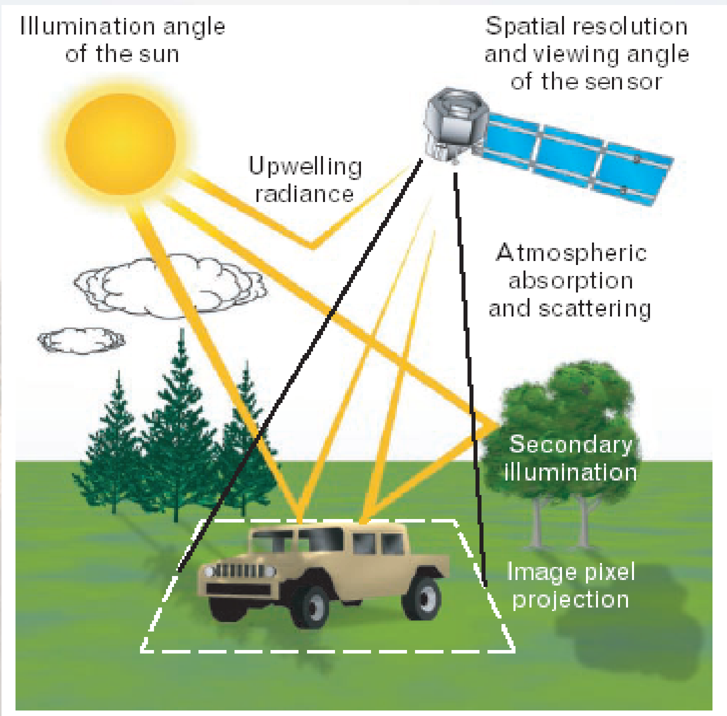

第四讲 红外辐射模型

(Infrared Radiation Models)

- VNIR和SWIR谱段辐射模型
- MWIR和TIR谱段辐射模型
- **红外辐射模型的拓展：空中目标的红外辐射建模**

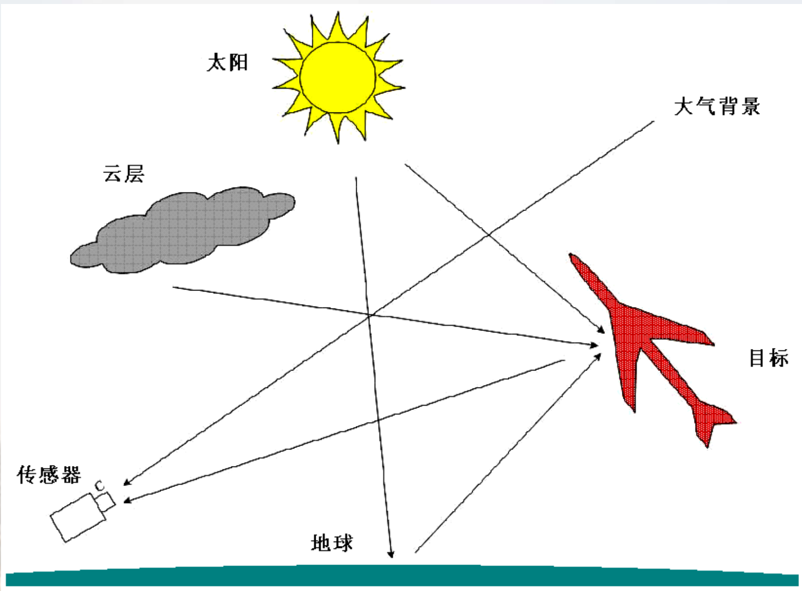

辐射光源：

- 太阳是主要的直射点光源；
- 太阳在地球、云层上反射的辐射照射到目标表面，再通过目标反射进入观测传感器的视野中；太阳对目标的加热；
- 大地本身由于太阳加温，自身温度升高并向外进行辐射。

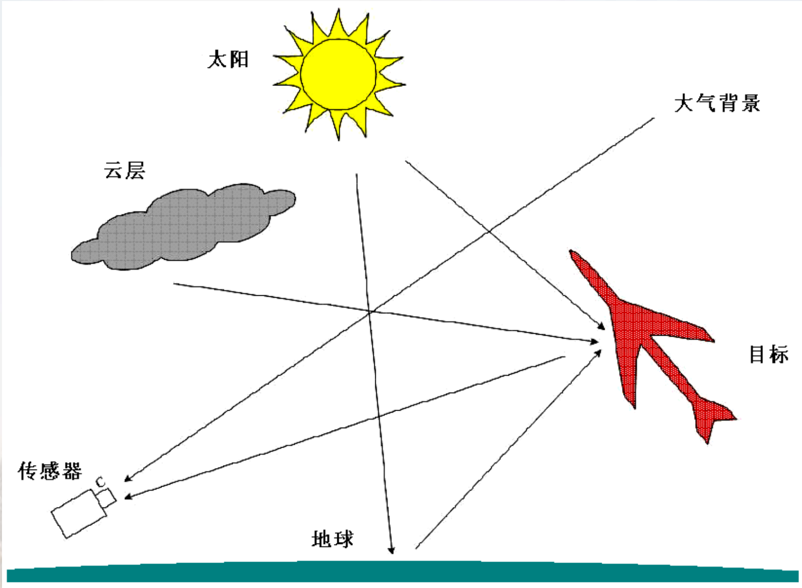

背景和大气路径：

- 大气背景辐射：大气对太阳光的散射所产生的辐射，包括背景和前景辐射；
- 红外辐射在大气中产生衰减和散射；
- 在太阳、云层、地面和目标之间的多种大气传播路径上，要依据大气中的天气现象和传播距离等因素计算辐射和衰减。

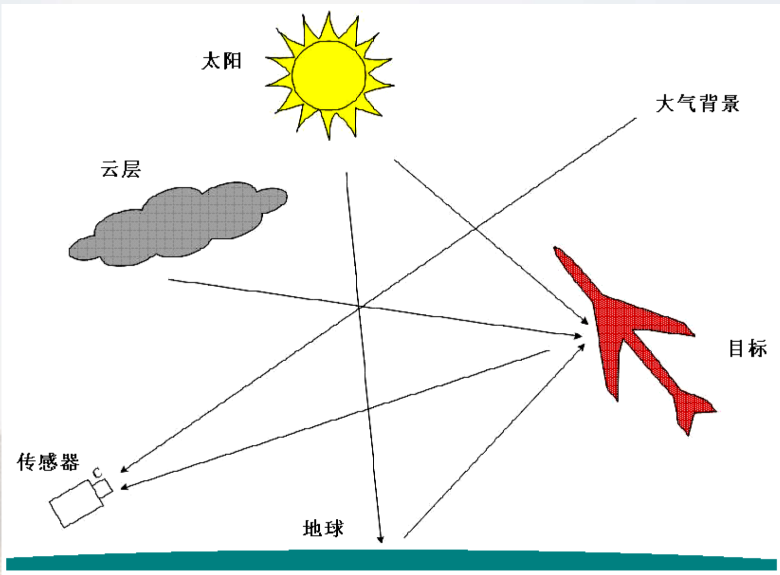

目标：

- 目标蒙皮的反射：目标接收来自外部光源的照射并向观测方向反射，包括来自太阳、天空和地海等背景辐射的反射辐射；
- 运动目标的空气动力加热，由于空中目标在高速运行中与空气磨擦产生的热辐射；
- 热部件：发动机燃烧等热部件向外传导的热量对表皮进行加热温产生的热辐射；
- 尾喷焰：尾喷流中水、二氧化碳、一氧化碳和碳粒等燃烧气体。

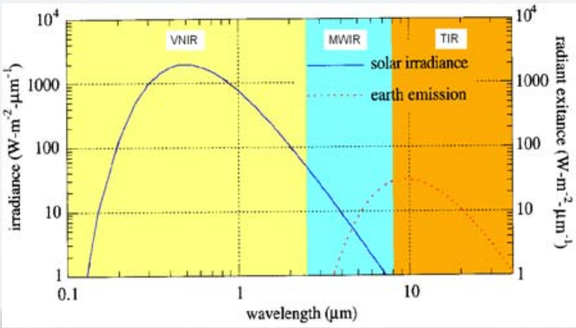

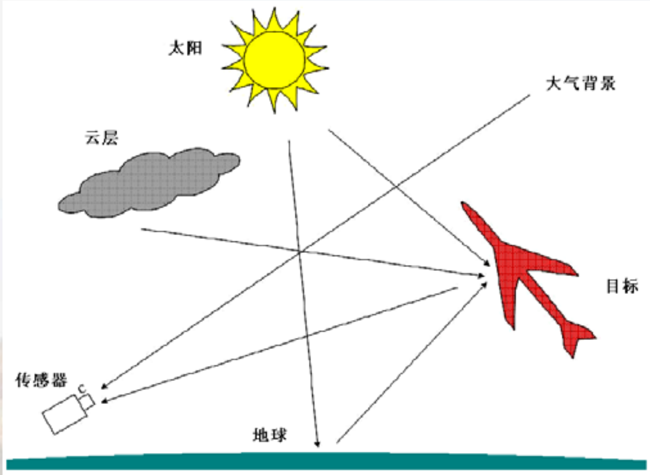

目标蒙皮的反射：

- 反射的太阳光谱辐射主要在VNIR、SWIR和MWIR波段
- 对地面和云层热辐射的反射主要在TIR和MWIR波段

蒙皮的反射和BRDF模型参数：

- 太阳、飞机和观察者之间的角度；
- 反射表面的形状；
- 反射类型，即漫射或镜面反射；
- 表面反射率大小；

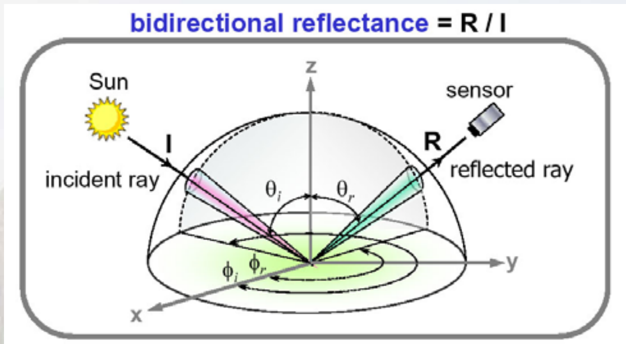

$$\rho(\theta_i,\varphi,\theta_r,\varphi_r)=\rho_d[(1-\beta)\cdot\delta(\theta_i,\theta_r)\cdot\delta(\varphi_i,\varphi_r\pm\pi)+\frac{\beta}{\pi}]$$

双向反射率　　理想的镜面反射　　理想的漫反射

蒙皮温度和辐射:

热平衡方程：

$$\rho c\delta\cdot dT_{\infty}/dt=-\varepsilon\sigma T_{\infty}^{4}+\alpha_{a}(T_{r}-T_{\infty})+\beta S$$

蒙皮向飞机内部的传导热流　　蒙皮的辐射热流　　气动加热热流　　太阳向蒙皮的辐射热流

将换热过程视为达到平衡态，即左边为零，解此方程可得出蒙皮的温度分布场

普朗克方程：

$$N_{\lambda}=\varepsilon(\lambda)\cdot N_{\lambda}^{0}(T)$$

成像传感器的红外图像

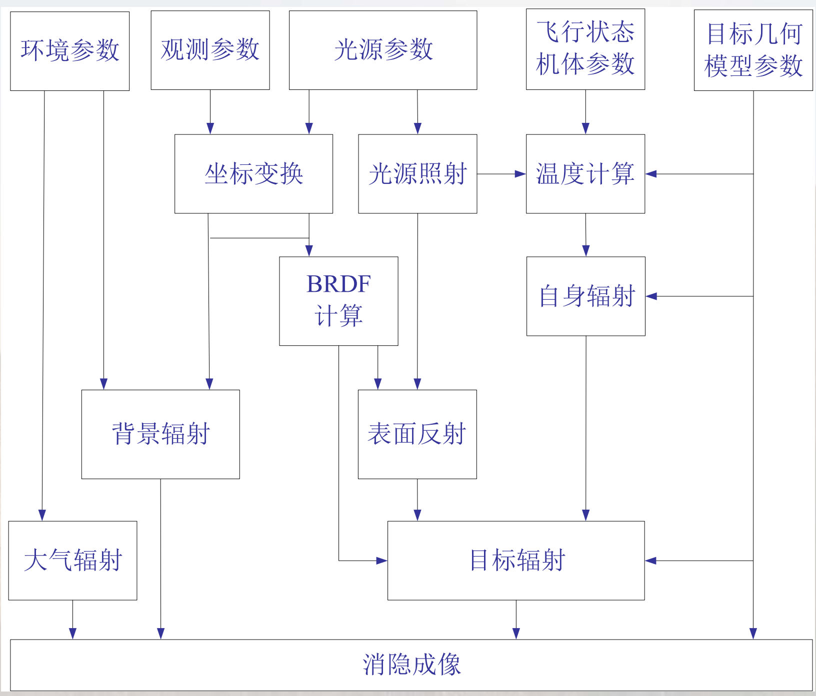

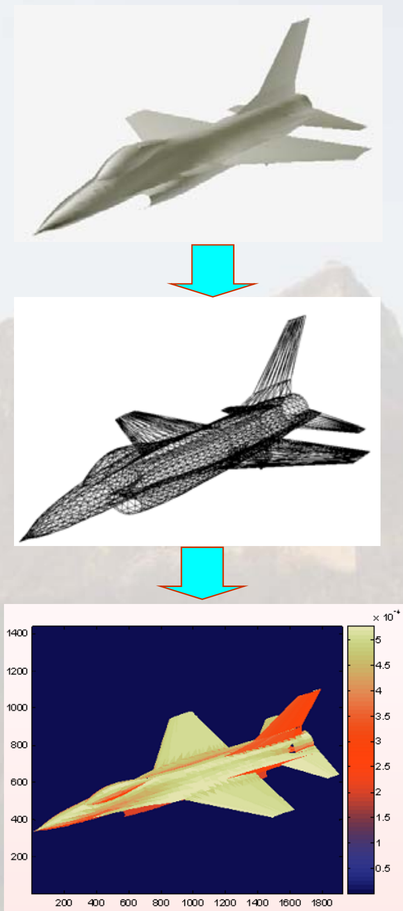

思考与拓展思考题

弹道导弹在助推段、中段和再入段全程的红外辐射特性主要受哪些因素的影响？

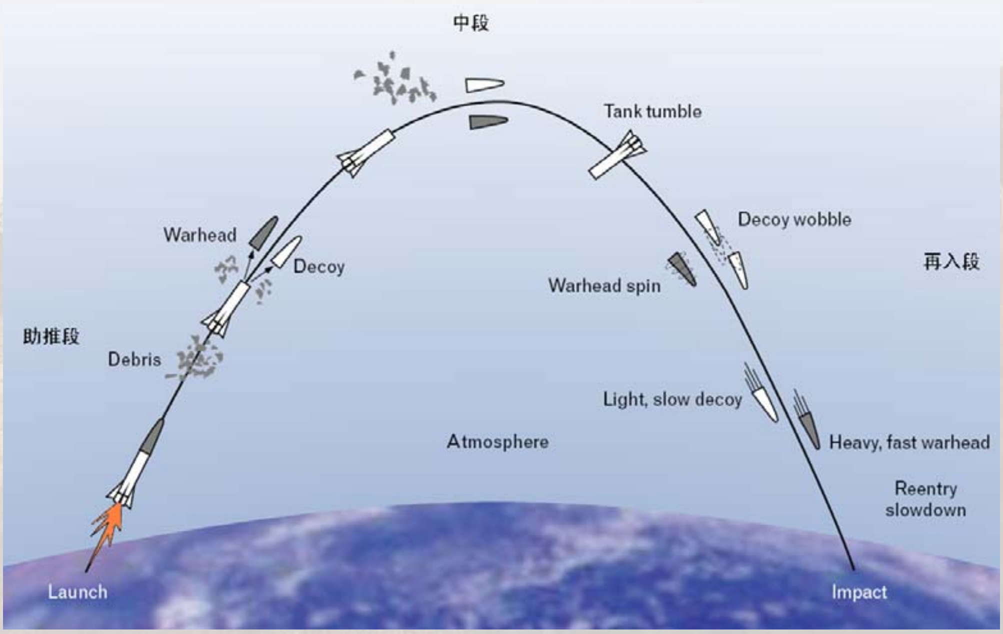

谢谢，请批评指正

许小剑
北京航空航天大学电子信息工程学院
Tel：13520723473
Email: xiaojianxu@buaa.edu.cn